UNIVERSITY
OF TRENTO

DIPARTIMENTO DI INGEGNERIA E SCIENZA DELL'INFORMAZIONE

38123 Povo – Trento (Italy), Via Sommarive 14
http://www.disi.unitn.it

INVERSION OF PHASELESS TOTAL FIELD DATA USING A TWO-STEP STRATEGY BASED ON THE ITERATIVE MULTI-SCALING APPROACH

G. Franceschini, M. Donelli, R. Azaro, and A. Massa

January 2011

Technical Report # DISI-11-075

Inversion of Phaseless Total Field Data using a Two-Step Strategy based on the Iterative Multi-Scaling Approach

Gabriele Franceschini, Massimo Donelli, Renzo Azaro, and Andrea Massa

Department of Information and Communication Technologies,

University of Trento, Via Sommarive 14, I-38050 Trento - Italy

Tel. +39 0461 882057, Fax +39 0461 882093

E-mail: *andrea.massa@ing.unitn.it*,

　　　{gabriele.franceschini, massimo.donelli, renzo.azaro} @dit.unitn.it

Web-page: *http://www.eledia.ing.unitn.it*

Inversion of Phaseless Total Field Data using a Two-Step Strategy based on the Iterative Multi-Scaling Approach

Gabriele Franceschini, Massimo Donelli, Renzo Azaro, and Andrea Massa

Abstract

In this paper, a new approach for the quantitative electromagnetic imaging of unknown scatterers located in free-space from amplitude-only measurements of the total field is proposed and discussed. The reconstruction procedure splits the problem into two steps. The method is based on the use of an inverse source algorithm to first complete the scattering data by estimating the distribution of the radiated field in the investigation domain. The object's function profile is then retrieved from the phaseless data via an iterative multiresolution procedure integrated with an effective minimization technique based on the particle swarm algorithm. Numerical examples are provided to assess the effectiveness of the whole two-step strategy in the presence of synthetic noise-corrupted data as well as in dealing with experimental datasets. Comparison with full-data and "bare" approaches are reported, as well.

Index Terms - Inverse Scattering, Electromagnetic Imaging, Phaseless Data, Integrated Multi-Scaling Approach, Particle Swarm Optimizer.

1 Introduction

In the last years, the interest in microwave imaging techniques is growing thanks to their sensitivity to the dielectric properties useful for detecting and reconstructing unknown objects in a non-invasive fashion. As a matter of fact, the reconstruction of the geometrical and physical characteristics of an unknown object is a key-issue in several applications concerned with non-destructive tests and evaluations [1][2] in the framework of applied geophysics [3][4], biomedical and industrial diagnostics [5]-[8] or subsurface sensing [9]. Nevertheless, although the effectiveness of these techniques for diagnostic purposes makes them very appealing, several open issues still remain partially solved or unsolved. Such an event gives rise to some doubts on the possibility of their large diffusion because of their intrinsic complexity.

From the scientific literature (see [10] and the references cited therein for a detailed overview), it is well known that the main drawbacks are due to the ill-posedness and the non-linear nature of the arising inverse scattering mathematical models.

On the other hand, for achieving a suitable resolution level in the reconstruction of the object profile, a non-negligible amount of information is necessary. Towards this purpose, multi-illumination [12] and/or multi-view [13] and/or multi-frequency systems [14] are generally used, but the information collectable from the scattering experiments still remain limited [10] to an upper bound that depends on the geometrical characteristics of the imaging system [15] even though some *a-priori* information (when available) on the scenario under test [16][17] or a set of constraints [18] on the retrievable dielectric profile are imposed. Therefore, various multiresolution strategies able to distribute in a non-uniform fashion the unknowns inside the scattering domain have been recently proposed (see [9], [19]-[25] for a detailed analysis) for overcoming the mismatch between number of scattering data and set of unknowns.

Besides the intrinsic drawbacks concerned with the mathematical model of an inverse problem, there are others practical issues related to the realization of low-cost and effective acquisition setups. As a matter of fact, while the amplitude measurement is not a critical point, the measurement of the phase of the scattered field turns out to be very difficult or very expensive in several applications and/or conditions. Although from a theoretical

point-of-view such a measure is not complicated at microwave and lower frequencies, the use of amplitude-only data notably simplifies the imaging setup and it allows a non-negligible reduction of costs.

On the other hand, by considering frequencies beyond tens of gigahertz, the direct measurement of the distribution of the phase of the electromagnetic field becomes harder and harder. Moreover, holographic and interferometric techniques, usually used in optical applications [26][27] for determining phase information, are experimentally demanding and often require an expensive post-processing of the measured data.

In order to avoid such drawbacks, some alternatives approaches have been proposed. Two main paths of research seem to be usually taken into account:

- the direct application of a reconstruction algorithm for the processing of phaseless field data (*Single-Step* Strategy) (see for example [28]-[31]);

- the splitting of the phaseless-data reconstruction into a two-step process (*Two-Step* Strategy) where the first step deals with a phase-retrieval problem for completing the amplitude-only inversion data and the latter is concerned with a standard reconstruction from complete field data (see for example [32][33]).

More in detail, in the framework of approximate methodologies for weak scatterers, Maleki *et al.* [28] proposed a single-step tomographic reconstruction procedure for determining the complex-valued index-of-refraction of inhomogeneous objects from the far-field intensity patterns generated by the scatterers in a sequence of scattering experiments. The same authors applied in [32] an alternative two-step methods based on an iterative phase-retrieval algorithm to extract the phase of the scattered field from the measurement of the amplitude of the total field and from *a-priori* information on the object support.

Unlike methods based on Born approximations, a complete single-step approach has been presented by Takenaka *et al.* in [29] for the reconstruction of the refractive index of unknown objects from intensity-only far-field data. Although based on a complete formulation of the scattering problem, likewise the approach in [32], such an approach requires some *a-priori* knowledge on the object support and in particular on its outer boundary. Still in the framework of single-step nonlinearized techniques, an iterative approach based on a memetic algorithm has been described in [31] dealing with dielectric multilayer

elliptic cylinders has been used. On the other hand, in [30], the minimization of the two-component discrepancy function is performed by means of the binary-constrained modified gradient method for detecting buried cylindrical homogeneous targets.

As far as two-step strategies are concerned, Isernia *et al.* proposed in [33] an innovative algorithm for better controlling the non-linearity with respect to single-step strategies through a convenient exploitation of the theoretical results on the inversion of quadratic operators.

The approach presented in this paper has several common and complementary features with respect to the above techniques. As a matter of fact, the proposed strategy is a two-step procedure where, nevertheless, the first step is not aimed at completing the amplitude-only scattering data, but at determining the input data for the so-called state equation for phaseless inputs. Furthermore, the second step is not concerned with a classical full-data inverse scattering problem, but it deals with a phaseless-data reconstruction through a suitable multi-scaling algorithm in order to fully exploit the limited amount of collectable information. To the best of the authors' knowledge, such a two-step retrieval process is completely innovative in the framework of intensity-only methods and it requires only the measurement of the scattering data in a limited number of locations in observation domain notably simplifying the collection-data process both in terms of measurement setup and acquisition time.

The paper is organized into four sections. The geometry of the problem and the general architecture of the proposed two-step strategy are described in Section 2. The results of a selected set of experiments are discussed in Section 3. Finally, Section 4 presents a discussion and some conclusions.

2   Mathematical Formulation

Let us consider a classical tomographic microwave imaging problem where an unknown cylindrical object located in an inaccessible investigation domain D_{inv} is illuminated at a fixed working frequency f by a set of V *TM*-polarized incident electromagnetic waves characterized by electric fields $\underline{E}_{inc}^{v}(\underline{r}) = E_{inc}^{v}(x, y)\widehat{z}$, $v = 1, ..., V$ (Figure 1).

For a *Full-Data* (FD) formulation, the scattered fields $E_{scatt}^{v} = E_{tot}^{v} - E_{inc}^{v}$, $v = 1, ..., V$, are

collected in $M^{(v)}$ measurement locations $[\left(x_{m(v)}, y_{m(v)}\right), m(v) = 1, ..., M(v), v = 1, ..., V]$ placed in an observation domain D_{obs} external to D_{inv} [13] and the inversion process is aimed at reconstructing the object function $\tau(x, y)$ defined as follows

$$\tau(x, y) = [\varepsilon_r(x, y) - 1] - j\frac{\sigma(x, y)}{2\pi f\epsilon_0} \quad (x, y) \in D_{inv} \tag{1}$$

ε_r and σ being the relative dielectric permittivity and the electric conductivity, starting from the knowledge in amplitude and phase of $E_{inc}^v(x, y)$, $(x, y) \in D_{inv}$, and $E_{scatt}^v\left(x_{m(v)}, y_{m(v)}\right)$, $\left(x_{m(v)}, y_{m(v)}\right) \in D_{obs}$. Towards this purpose and according to the description of the scattering phenomena in terms of the Fredholm formalism [?], the following equations are formulated and solved

$$E_{scatt}^v\left(x_{m(v)}, y_{m(v)}\right) = -j\frac{k_0^2}{4} \int\int_S \tau(x', y')E_{tot}^v(x', y')H_0^{(2)}(k_0 d)\, dx' dy' \quad \left(x_{m(v)}, y_{m(v)}\right) \in D_{obs} \tag{2}$$

$$E_{inc}^v(x, y) = E_{tot}^v(x, y) + j\frac{k_0^2}{4} \int\int_S \tau(x', y')E_{tot}^v(x', y')H_0^{(2)}(k_0 d)\, dx' dy' \quad (x, y) \in D_{inv} \tag{3}$$

where k_0 is the free-space wavenumber, $H_0^{(2)}$ is the 0-*th* order second-kind Hankel function, and $d = \sqrt{(x - x')^2 + (y - y')^2}$.

Unlike *FD* approach, let us consider a "phaseless data" (PD) inversion where only the amplitude of the total field in the observation domain, $\left|E_{tot}^v\left(x_{m(v)}, y_{m(v)}\right)\right|$, $\left(x_{m(v)}, y_{m(v)}\right) \in D_{obs}$, $m(v) = 1, ..., M(v)$, $v = 1, ..., V$, and of the amplitude of the incident field in N locations of the investigation domain, $|E_{inc}^v(x_n, y_n)|$, $(x_n, y_n) \in D_{inv}$, $n = 1, ..., N$, are available. Under these hypotheses, the system of equations (2)-(3) is modified as follows

$$\left|E_{tot}^v\left(x_{m(v)}, y_{m(v)}\right)\right| = \left|E_{inc}^v\left(x_{m(v)}, y_{m(v)}\right) - j\frac{k_0^2}{4} \int \int_S \tau(x', y')E_{tot}^v(x', y')H_0^{(2)}(k_0 d_{m(v)})\, dx' dy'\right|$$
$$\left(x_{m(v)}, y_{m(v)}\right) \in D_{obs} \tag{4}$$

$$|E_{inc}^v(x_n, y_n)| = \left| E_{tot}^v(x_n, y_n) + j\frac{k_0^2}{4} \int\int_S \tau(x', y') E_{tot}^v(x', y') H_0^{(2)}(k_0 d_n)\, dx' dy' \right| \quad (x_n, y_n) \in D_{inv} \tag{5}$$

As can be noticed, while the mathematical formulation of the *PD* problem does not notably differ from that concerned with the *FD* case, certainly the use of intensity-only data turns out in a further reduction of the collectable information on the scenario under test with respect to that already limited in the *FD* situation. Therefore, even more so in the case of phaseless data, the use of an adaptive multi-resolution strategy seems to be even more mandatory in order to fully and effectively exploit the limited amount of available information for achieving a suitable accuracy in the reconstruction. Towards this end, a customized version of the iterative multi-scaling approach (*IMSA*) can be profitably used.

The application of the *IMSA* approach to phaseless data requires at each step s ($s = 1, ..., S$) of the multi-step procedure the minimization of the following multi-resolution cost function[1]

$$\Phi^{(s)} \left\{ \tau\left(x_{n(r)}, y_{n(r)}\right), E_{tot}^v\left(x_{n(r)}, y_{n(r)}\right); \begin{array}{c} v = 1, ..., V \\ n_{(r)} = 1, ..., N_{(r)} \quad r = 1, ..., s \end{array} \right\} = \Phi_{Data}^{(s)} + \Phi_{State}^{(s)} \tag{6}$$

$$\Phi_{Data}^{(s)} = \frac{\displaystyle\sum_{v=1}^{V}\sum_{m(v)=1}^{M(v)} \left| \left| E_{tot}^v\left(x_{m(v)}, y_{m(v)}\right) \right| - \left| \xi_{tot}^v\left(x_{m(v)}, y_{m(v)}\right) \right| \right|^2}{\displaystyle\sum_{v=1}^{V}\sum_{m(v)=1}^{M(v)} \left| E_{tot}^v\left(x_{m(v)}, y_{m(v)}\right) \right|^2}$$

$$\Phi_{State}^{(s)} = \frac{\displaystyle\sum_{v=1}^{V}\sum_{r=1}^{s}\sum_{n(r)=1}^{N(r)} \left| \left| E_{inc}^v\left(x_{n(r)}, y_{n(r)}\right) \right| - \left| \xi_{inc}^v\left(x_{n(r)}, y_{n(r)}\right) \right| \right|^2}{\displaystyle\sum_{v=1}^{V}\sum_{r=1}^{s}\sum_{n(r)=1}^{N(r)} \left| E_{inc}^v\left(x_{n(r)}, y_{n(r)}\right) \right|^2}$$

where

---

[1] Such a discretized form has been obtained by applying the Richmond's [34] procedure to the system of equations (4)-(5).

$$\left| \xi_{tot}^v \left(x_{m(v)}, y_{m(v)} \right) \right| = \left| E_{inc}^v \left(x_{m(v)}, y_{m(v)} \right) + \sum_{r=1}^{s} \sum_{n(r)=1}^{N(r)} \left\{ \omega_{n(r)}^{(s)} \left[\tau \left(x_{n(r)}, y_{n(r)} \right) E_{tot}^v \left(x_{n(r)}, y_{n(r)} \right) G_{m(v),n(r)} \right] \right\} \right|$$

(7)

$$\left| \xi_{inc}^v \left(x_{n(r)}, y_{n(r)} \right) \right| = \left| E_{tot}^v \left(x_{n(r)}, y_{n(r)} \right) - \sum_{t=0}^{s-1} \sum_{q(t)=1}^{N(r)} \left\{ \omega_{q(t)}^{(s)} \left[\tau \left(x_{q(t)}, y_{q(t)} \right) E_{tot}^v \left(x_{q(t)}, y_{q(t)} \right) G_{n(r),q(t)} \right] \right\} \right|$$

(8)

and $\omega_{n(r)}^{(s)}$ is the weighting function defined as

$$\omega_{n(r)}^{(s)} = \begin{cases} 0 & if \, r \neq s \, and \, \left(x_{n(r)}, y_{n(r)} \right) \notin D^{(s)} \\ 1 & if \, \left(x_{n(r)}, y_{n(r)} \right) \in D^{(s)} \end{cases}$$

(9)

r being the index of the resolution level and $D^{(s)}$ the Region of Interest (RoI) at the s-th step defined on the basis of the information collected by the reconstruction of the $(s-1)$-th iteration according to the procedure detailed in [22].

However, it should be noticed that such an implementation requires the knowledge of $\left| E_{inc}^v \left(x, y \right) \right|$ at different level of resolution with a step-by-step decreasing of the sampling interval. From a practical point of view, the measure of $\left| E_{inc}^v \left(x, y \right) \right|$ is generally carried out in a limited number of measurement points $\left[\left(x_n, y_n \right), n = 1, ..., N \right]$ in D_{inv} although theoretically it could be performed in whatever location of the investigation domain. Nevertheless, the experimental system (and in particular the electromagnetic sensors) is moved by means of a mechanical apparatus with some tolerances in the positioning (which strongly depends on the application, but generally it is of the order of millimeters [5]). Therefore, a reduced sampling distance between adjacent positions in D_{inv} would result in an inaccurate measure of the field and, consequently, each measured sample would be corrupted by a non-negligible error.

Because of such a drawback, there is the need of defining a suitable model of the radiating source in order to apply an iterative multi-resolution strategy and thus for computing the radiated field in whatever position of the investigation domain. Towards this end, avoiding the measurement of $\left| E_{inc}^v \left(x_n, y_n \right) \right|$, $\left(x_n, y_n \right) \in D_{inv}$, some alternative information on the radiated field are necessary. Therefore, let us suppose that the knowledge of the incident field radiated by the electromagnetic source is available both in amplitude and phase in the observation domain, $E_{inc}^v \left(x_{m(v)}, y_{m(v)} \right)$, $\left(x_{m(v)}, y_{m(v)} \right) \in D_{obs}$. Such an assumption is

generally verified in real situations as confirmed by the laboratory-controlled experiments carried out at the *Centre Commun de Ressources Micro-ondes* (*CCRM*) in Marseille [35][36]. As a matter of fact, such an evaluation can be performed only once and off-line (i.e., non during the imaging process of an unknown object) for each measurement system (i.e., the measurement setup constituted by the illuminating source and the receivers) and in a non-so-expensive and accurate fashion for a reduced number of adequately-spaced locations. Furthermore, unlike the measurement in D_{inv}, the measurement locations in D_{obs} are not so close the one to the others and they are in a small number if chosen according to the "golden rule" defined in [15].

According to these idea, the inversion process turns out to be carried out through the two-step strategy schematized in Fig. 2 and detailed in the following.

Step 1 - Source Synthesis

Let us assume that, because of the complexity and difficulties in collecting reliable and independent measures in a dense grid of points, the incident field is only available at the measurement points belonging to the observation domain $[E_{inc}^v \left(x_{m(v)}, y_{m(v)} \right), \left(x_{m(v)}, y_{m(v)} \right) \in D_{obs}]$. Therefore, in order to apply the constraints stated through the "State" equation (5) and before facing with the data inversion, it is mandatory to develop a suitable model able to predict the incident field radiated by the actual electromagnetic source in the investigation domain D_{inv}.

Towards this aim, let us consider the so-called *Distributed-Cylindrical-Waves Model* (proposed and validated in [37] when dealing with experimental) where the actual source is represented by a linear array of W equally-spaced line-sources, which radiates an electric field given by

$$\widetilde{E}_{inc}^v \left(x, y \right) = -\frac{k_0^2}{8\pi f \varepsilon_0} \sum_{w=1}^{W} A \left(x_w, y_w \right) H_0^{(2)} \left(k_0 d_w \right) \tag{10}$$

where $A(x_w, y_w)$ is the unknown coefficient related to the w-*th* element of the array. Such a model is completely defined when the set of unknown coefficients, $\underline{\mathbf{A}} = \{A(x_w, y_w), w = 1, ..., W\}$, is determined starting from the knowledge of the incident field measured

9

in the observation domain through the solution of the following problem

$$\underline{\mathbf{A}}_{opt} = arg \left\{ min_{\underline{\mathbf{A}}} \left(\frac{\sum_{v=1}^{V} \left\| \underline{E}_{inc}^v - \widetilde{\underline{E}_{inc}^v} \right\|^2}{\sum_{v=1}^{V} \left\| \underline{E}_{inc}^v \right\|^2} \right) \right\} \tag{11}$$

where $\underline{E}_{inc}^v$ is an array of the measures collected for the v-th view at $M(v)$ measurement points of the observation domain whose $m(v)$-th element is equal to $E_{inc}^v \left(x_{m_{(v)}}, y_{m_{(v)}} \right)$; $\widetilde{\underline{E}_{inc}^v}$ is the array of numerically-computed values of the incident field in the observation domain given by $\widetilde{\underline{E}_{inc}^v} = [\mathcal{G}] \underline{A}$, $[\mathcal{G}]$ being a $W \times M(v)$ matrix whose generic element is equal to $G_{m(v),w} = -\frac{k_0^2}{8\pi f \varepsilon_0} H_0^{(2)} \left(k_0 d_{m(v),w} \right)$.

Unfortunately, (11) involves the limitations of an inverse-source problem, that is $[\mathcal{G}]$ is ill-conditioned and the solution is usually non-stable and non-unique. In order to overcome such a drawback, the solution of (11) is recast as the inversion of the linear operator $[\mathcal{G}]$ through a SVD-decomposition [38] by looking for the optimal configuration $\underline{\mathbf{A}}_{opt}$ that provides the optimal matching between measured and numerically-computed values of the incident field in the observation domain

$$\underline{\mathbf{A}}_{opt} = arg \left\{ min_W \left(\frac{\sum_{v=1}^{V} \left\| \left\{ \underline{\Omega}_v \left[\Gamma_v \right]^{-1} \underline{\Theta}_v^* \right\} \underline{E}_{inc}^v \right\|^2}{\sum_{v=1}^{V} \left\| \underline{E}_{inc}^v \right\|^2} \right) \right\} \tag{12}$$

where $\underline{\Omega}_v$ and $\underline{\Theta}_v$ are isometric matrices, $(^*)$ denotes the adjoint operator, and $[\Gamma_v]$ is a diagonal matrix whose positive diagonal elements are the singular values of $[\mathcal{G}]$ [10].

Step 2 - Object Function Reconstruction

Following the general architecture of the multi-step procedure detailed in [21] for the FD problem, the IMSA is applied to the phaseless data problem by repeating the following procedural operations until the termination conditions hold true [22]:

- **Data Computation**

  Starting from the modeling of the electromagnetic source derived at the "*Step 1*" with the determination of $\underline{\mathbf{A}}_{opt}$, compute $\left| \widetilde{E}_{inc}^v \left(x_{n(r)}, y_{n(r)} \right) \right|$, $\left(x_{n(r)}, y_{n(r)} \right) \in D_{inv}$, $n(r) = 1, ..., N(r)$, $r = s$, through Eq. (10);

- **Retrieval Process**

Minimize the multi-resolution cost function $\widetilde{\Phi}^{(s)}$ defined as follows

$$\widetilde{\Phi}^{(s)} = \Phi^{(s)}_{Data} + \widetilde{\Phi}^{(s)}_{State} \tag{13}$$

being

$$\widetilde{\Phi}^{(s)}_{State} = \frac{\sum_{v=1}^{V}\sum_{r=1}^{s}\sum_{n(r)=1}^{N(r)} \left|\left|\widetilde{E}^{v}_{inc}\big(x_{n(r)}, y_{n(r)}\big)\right| - \left|\xi^{v}_{inc}\big(x_{n(r)}, y_{n(r)}\big)\right|\right|^{2}}{\sum_{v=1}^{V}\sum_{r=1}^{s}\sum_{n(r)=1}^{N(r)} \left|\widetilde{E}^{v}_{inc}\big(x_{n(r)}, y_{n(r)}\big)\right|^{2}}$$

by considering the multiresolution representation of the unknowns at the s-th step $\left\{\tau\left(x_{n(r)}, y_{n(r)}\right),\ E^{v}_{tot}\left(x_{n(r)}, y_{n(r)}\right);\ n(r) = 1, ..., N(r);\ r = 1, ..., s;\ v = 1, ..., V\right\}$ and according to the iterative *PSO*-based approach [11].

3   Numerical Validation

This section is aimed at presenting the results obtained during the testing and numerical validation of the two-step reconstruction strategy. After a short overview of the characteristics of the measurement setup and of the scenario conditions that we followed in our study, several experiments are presented in order to: (a) assess the effectiveness and current limitations of the proposed *PD* approach in various environmental conditions and scatterers configurations; (b) compare the obtained results with those reached exploiting the information contained in both amplitude and phase of the scattered field (*FD* approach) both qualitatively, in terms of dielectric profile maps, and quantitatively, in terms of the reconstruction errors as defined in [21]. Towards these purposes and in order to better understand and appreciate the usefulness of the implemented phaseless-data strategy, two meaningful classes of test cases are considered. The first one deals with synthetic examples where scattering data are corrupted with different levels of an additive Gaussian noise (defined as in [22]) for evaluating the robustness of the approach. While the second one is concerned with some of the experimental datasets of the "*Marseille*" database [35][36].

3.1 Synthetic Assessment

The first step of the numerical assessment deals with synthetic test cases for which scattering data are user-defined (thus controlled) as well as the sources of noise.

In all the following examples, the unknown scatterers belong to a square investigation domain of side $L_{inv} = 2\,\lambda$ and they are illuminated by plane waves impinging from $V = 32$ equally-spaced directions $[\theta^v = 2\pi\frac{(v-1)}{V}, v = 1, ..., V]$. The observation domain is a circle $R_{obs} = 5\,\lambda$ in radius and the scattering data are computed in $M(v) = 32$, $v = 1, ..., V$, measurement points equally-distributed along D_{obs}.

As far as the *PSO*-based method for the "*retrieval process*" is concerned, the following configuration of parameters has been adopted according to the guidelines in the related literature [39][40] and to the heuristic study carried out in [11]: $w = 0.4$ (constant inertial weight), $I = \frac{5}{100}U$ (swarm dimension, U being the number of problem unknowns), and $C_1 = C_2 = 2.0$ (acceleration coefficients). Moreover, the IMSA has been used with the parameters setting defined in [22].

In the first example, the scatterer is a centered ($x_{ref} = x_{RoI} = 0.0$, $y_{ref} = y_{RoI} = 0.0$) homogeneous dielectric ($\tau_{ref} = 1.0$) square cylinder $L_{ref} = L_{RoI} = \frac{\lambda}{2}$ sided. After solving the "*source-synthesis*" step, the array coefficients turned out to be distributed as shown in Fig. 3. Such a configuration can be considered optimal in terms of the matching with problem data as requested by (12). In order to give an idea of the fitting between "measured" and estimated data, Figure 4 shows the values of the amplitudes and phases of the radiated-fields in D_{obs} for $v = 1$. As can be seen, an accurate reconstruction is achieved both in amplitude [Fig. 4(a)] and phase [Fig. 4(b)]. Similar conclusions hold true for all incidence angles.

Starting from the estimated model of the source, the "*object-function reconstruction*" has been carried out applying the iterative multi-scaling approach. In Fig. 5, processing results at various stages through the multi-step reconstruction are shown. As a reference, the ideal reconstruction is displayed in [Fig. 5(a)]. For comparison purposes, the profile estimated with the *FD* approach is reported in Fig. 5(e), as well. As it can be observed, the scatterer appears fairly well retrieved by the *IMSA*, be this inversion led with or without the phase information (Tab. I). The corresponding object-function maps illustrate

that, whatever the approach, both a good location and shape retrieval are obtained. The only difference comes from the fact that the PD inversion slightly shifts the location of the object with respect to its real position as confirmed by the value of the localization error $(\rho^{(PD)}\big|_{S=3} = 2.80$ vs. $\rho^{(FD)}\big|_{S=3} = 0.02)$. In order to further confirm the similar behavior of the two approaches, let us consider the distribution of the scattered field in the observation domain (Fig. 6) as a similarity index.

For completeness and in order to point out the effectiveness of the optimization approach based on the PSO algorithm [11], Figure 7 gives an indication of the fitting between actual and estimated data both in D_{obs} [Fig. 7(a)] and in the RoI at different steps of the reconstruction process [e.g., $(r = 0)$ indicates the locations in D_{ind} that belong to the RoI estimated at $(s = 1)$].

The last experiment of this synthetic test case is aimed at evaluating the robustness of the two-step PD approach to the presence of the noise in the inversion data. In order to benchmark how the "*two-step*" strategy adapts to a changing environment, different amounts of gaussian noise [22] have been added to $\left| E_{tot}^{v}\left(x_{m(v)}, y_{m(v)}\right) \right|$, $\left(x_{m(v)}, y_{m(v)}\right) \in D_{obs}$.

Figure 8 shows the evolution through different signal-to-noise ratios (SNRs) of the error indexes. The SNR has been varied between $5\,dB$ and $40\,dB$ and 100 realizations were averaged for each value, which constitutes a reasonable confidence margin for a statistic evaluation. As expected, the FD approach yields the best results through the whole signal-to-noise domain. It is also noticeable that the differences between FD and PD reduces when the noise level increases indicating a significant impact of the noise especially in the phase information. Moreover, since both qualitative and quantitative error figures assume similar values for non-negligible noise levels, it seems to indicate that the PD strategy could be profitably adopted in such conditions because of the favorable trade-off between accuracy and simplicity of the imaging setup with respect to a FD methodology. Similar results hold true for other test cases. As an example, let us observe the estimated profiles [Figs. 9(c)-9(d)] when $SNR = 20\,dB$ and the scattering scenario is that shown in [Figs. 9(a)-9(b)].

3.2 Experimental Assessment

In the light of the acceptable results obtained in dealing with synthetic data corrupted by various amounts of an additive noise and simulating real situations (where real-time acquired phaseless data are subject to temperature and/or humidity variations, measurement noise at the sensors, observation noise, etc.), the "*two-step*" strategy has been assessed facing the real scattering data kindly provided by M. Saillard and K. Belkebir [35][36].

As far as the PD approach is concerned, even though the knowledge of the total field in D_{obs} was available both in phase and amplitude, only the amplitude has been used. Moreover, the laboratory-acquired measures of $E_{inc}^v\left(x_{m(v)},\,y_{m(v)}\right)$, $\left(x_{m(v)},y_{m(v)}\right) \in D_{obs}$, have been considered for defining the model of the actual source.

The first test case considers the so-called "*dielTM_ dec8f.exp*" scattering configuration [35], which consists of a homogeneous dielectric ($\tau_{ref} = 2.0 \pm 0.3$) cylinder of radius $\frac{L_{RoI}}{2} = 1.5 \times 10^{-2}\,[mt]$ located in an off-centered position ($x_{ref} = x_{RoI} = 0.0$, $y_{ref} = y_{RoI} = -3.0 \times 10^{-2}\,[mt]$) in the investigation domain ($L_{inv} = 30.0 \times 10^{-2}\,[mt]$) where the scatterer is assumed to lie. Because of the aspect-limited nature of the acquisition setup, the complete set of measures $[M(v) = 49,\, v = 1, ..., V,\, V = 36]$ collected in a circle $R_{obs} = 76.1 \times 10^{-2}\,[mt]$ in radius has been used, but only mono-frequency data have been considered.

In the first experiment, the reconstruction has been carried out at the working frequency of $f = 1\,GHz$. Moreover, different methods considering both complex and amplitude-only data have been used for allowing an exhaustive comparative analysis.

Let us consider the retrieved dielectric maps obtained with PD through the "*bare*"[2] PSO-based approach [Fig. 10(a)] and the $IMSA$-PSO strategy [Fig. 10(b)] described in this paper. Concerning the FD, we will show the results obtained with stochastic [the "*bare*" PSO-based approach - Fig. 10(c) - and the $IMSA$-PSO strategy [11] - Fig. 10(d)] as well as deterministic [the "*bare*" CG-based approach - Fig. 10(e) - and the $IMSA$-CG strategy [21] - Fig. 10(f)] optimization methods.

Let us observe the reconstructed profile shown in Fig. 10(b), even though some artifacts

---

[2] A single-step inversion where the whole investigation domain is discretized with a spatial sampling size equal to that reached in the RoI by the IMSA estimated at the convergence step.

are present and the image turns out partially smoothed, it is possible to distinguish the shape and infer the position of the actual object. On the contrary, neither the location nor the shape of the scatterer can be deducted from the reconstruction obtained through the PD "*bare*" PSO-based approach [Fig. $10(a)$].

By comparing these results with those of the FD approaches [Figs. $10(c)$-$10(f)$], some differences can be observed. As expected, the amplitude-only knowledge causes a reduction of the quality of the reconstruction with respect to a complete data inversion. However, it turns out that the retrieved profile through the "two-step" PD strategy is better than those of the single-step "*bare*" methods both using PD [Fig. $10(a)$] and FD [Fig. $10(c)$ and Fig. $10(e)$]. Moreover, it compares in an acceptable fashion with others $IMSA-FD$ methods as confirmed by the values reported in Tab. II. These considerations further point out the need of facing the lack of information (in this case, the phase of the field) with an effective use of that available by means of effective multiresolution methodologies. Therefore, whether in [21] the need of improving the achievable spatial resolution motivated the use of an $IMSA$ approach, it becomes essential for achieving a fair inversion when considering amplitude-only data.

Finally, in order to give some indications on the relationship between reconstruction accuracy and information content of the data, let us observe the plots of the fields that are produced by the inversion algorithm (different from those which could be derived by the retrieved dielectric map by solving the direct problem independently). The reason of a reduced accuracy in the reconstruction when dealing with PD cannot be ascribed to an unsatisfactory minimization of (13), since the fitting between actual and estimated scattering data is optimal at the convergence [Fig. 11]. It is certainly related to the information on the phase as indirectly pointed out in Fig. 12 where it is evident the mismatching between the amplitude of the scattered field estimated by using the retrieved profile with the PD approach and the actual one, whereas the FD algorithm suitably reproduces the reference plot.

The second experiment of this section is aimed at evaluating the impact of the phase information on the reconstruction at different frequencies. Towards this end, the datasets of the "Marseille" benchmark concerned with different frequencies from $1\,GHz$ up to

$8\,GHz$ have been processed.

Likewise the FD approaches, the effectiveness of PD methods in reconstructing the scatterer significantly reduces when the frequency increases as confirmed by the evolution of the localization error (Fig. 13). Moreover, by comparing the localization accuracies of the $IMSA$ approaches, it turns out that the difference between the error indexes (i.e., $\Theta = \rho^{(IMSA-PD)} - \rho^{(IMSA-FD)}$) enlarges as the frequency increases. Such a behavior clearly indicates the more and more negative effect in neglecting the phase information when higher frequencies are used for sensing the scatterer under test.

In order to show the capability of the proposed strategy in detecting and reconstructing layered structures, the last test case deals with a two-layer circular structure described in the new "Marseille" database [36] and denoted by the acronym "$FoamDielIntTM$". Such a scattering configuration is characterized by the following quantities: $\tau_{ref}^{(1)} = 2.0 \pm 0.3$, $L_{ref}^{(1)} = 1.5 \times 10^{-2}\,[mt]$, $\tau_{ref}^{(2)} = 0.45 \pm 0.15$ and $L_{ref}^{(2)} = 4.0 \times 10^{-2}\,[mt]$. As far as the imaging setup is concerned, the descriptive parameters are all the same as in the first experimental scattering database [35], except for the radius of the observation domain ($R_{obs} = 1.67\,[mt]$) and the number of views and measurement locations [$M(v) = 241$, $v = 1, ..., V$, $V = 8$]. For a detailed description of the measurement setup please see [41]. Taking into account previous results in dealing with dielectric obstacles, the dataset related to the lowest working frequency has been considered ($f = 2\,GHz$). Moreover, the same number of array elements used for the first example of this sub-section has been considered for modeling the actual source and computing their amplitudes by means of the SVD. Such a constraint has been imposed to verify the validity of the same source model for both the "Marseille" datasets as well as the dependence of the reconstruction on the accuracy of the equivalent source.

Even though the adopted source model faithfully reproduces the phase [Fig. 14(b)] of the radiated field in the observation domain, some deviations from the real data can be noticed in the corresponding amplitudes [Fig. 14(a)]. Such an event clearly indicates that the source modeling is not completely optimal. Starting from such source-synthesis, the results of the retrieval processes carried out with PD and FD approaches are shown in Fig. 15. Despite the approximate model of the radiating source, both the inversion performed

with the $IMSA - PD$ and with the $IMSA - FD$ lead to acceptable results. Although, the scatterer cannot be exactly identified, the algorithms converged to a structure that occupies a large subset of the true obstacle and both of them revealed the boundaries of the layers. In particular, it should be pointed out that the final reconstruction obtained by the "two-step" PD strategy is essentially almost identical to that one achieves starting from complete scattering data as confirmed by the values in Tab. III.

4   Conclusions

A two-step strategy based on amplitude-only measurements of the total field has been proposed and analyzed. The system architecture has been designed integrating the iterative multi-resolution reconstruction strategy with a source modeling technique to fully exploit the limited amount of information achievable from scattering data, without requiring expensive measurement setups or complex acquisition procedures.
The main features of the proposed strategy are the following:

- capability to exploit the limited amount of information achievable from amplitude-only measurements in an effective fashion by means of the use of a multi-scaling representation of the problems unknowns;

- capability to deal with complex nonlinear cost functions as well as the occurrence of possible false solutions (or local minima of the cost functional) thanks to the effectiveness of a distributed-intelligence optimization algorithm;

- robustness to common levels of noise.

Concerning the methodological novelties of this work, besides the definition of the global architecture of the whole system, some specific aspects should be pointed out:

- original two-step strategy that allows a reduced number of measures and external to the investigation domain;

- specific and innovative formulation of the amplitude-only data inversion within the framework of inverse scattering algorithms;

- use of a multi-resolution procedure to address the phaseless-data inversion;

- use of a particle swarm optimizer for the iterative minimization of the non-differentiable amplitude-only cost function.

In the numerical assessment carried out on different conditions and experimental datasets concerned with various scattering configurations, the proposed architecture proved effective, providing both acceptable reconstruction accuracy and robustness to the noise as well as to false solutions. Final reconstructions have usually shown a general agreement with those from full data (amplitude and phase) and actual profiles. As far as the information related to the phase value is concerned, the numerical results pointed out that phaseless inversions are very close and essentially identical to those obtained with a complete approach in the presence of non-negligible levels of noise (synthetic experiments) and for lower frequencies (experimental datasets).

Because of the favorable trade-off between complexity/costs of the acquisition setup and reconstruction effectiveness, the proposed approach seems a very promising tool to be used in industrial applications for non-destructive tests and evaluations. Towards this purpose, further developments of this research work will be oriented in two different directions:

1. further simplifying the required imaging system by developing a procedure that does not require the measure of the phase of the radiated field (even though in such a case it is limited to the observation domain and it can be performed once and off-line during the calibration of the measurement setup);

2. extending the two-step strategy from free-space configurations to layered/stratified media as well as inhomogeneous backgrounds for dealing with biomedical and more realistic industrial applications.

Acknowledgements

References

[1] J. Ch. Bolomey. *Frontiers in Industrial Process Tomographay*. Engineering Foundation, 1995.

[2] J. Ch. Bolomey, "Microwave imaging techniques for NDT and NDE," *Proc. Training Workshop on Advanced Microwave NDT/NDE Techniques*, Supelec/CNRS, Paris, Sep. 7-9, 1999.

[3] D. Goodman, "Ground penetrating radar simulation in engineering and archeology," *Geophysics*, vol. 59, pp. 224-232, 1994.

[4] A. C. Dubey *et al.*, *Detection technology for mines and minelike taragets*. Eds. Orlando, FL, 1995.

[5] A. Franchois, A. Joisel, Ch. Pichot, and J. Ch. Bolomey, "Quantitative microwave imaging with a 2.45 GHz planar microwave camera," *IEEE Trans. Medical Imaging*, vol. 17, pp. 550-561, Aug. 1998.

[6] X. Li, S. K. Davis, S. C. Hagness, D. W. van der Weide, and B. D. Van Veen, "Microwave imaging via space-time beamforming: experimental investigation of tumor detection in multilayer breast phantoms," *IEEE Trans. Microwave Theory Tech.*, vol. 52, pp. 1856-1865, Aug. 2004.

[7] Q. Fang, P. M. Meaney, and K. D. Paulsen, "Microwave imaging reconstruction of tissue property dispersion characteristics utilizing multiple-frequency informatio," *IEEE Trans. Microwave Theory Tech.*, vol. 52, pp. 1866-1875, Aug. 2004.

[8] S. Caorsi, A. Massa, M. Pastorino, and A. Rosani, "Microwave medical imaging: potentialities and limitations of a stochastic optimization technique," *IEEE Trans. Microwave Theory Tech.*, vol. 52, pp. 1908-1916, Aug. 2004.

[9] O. M. Bucci, L. Crocco, T. Isernia, and V. Pascazio, "Suabsurface inverse scattering problems: Quantifying qualifying and achieving the available information," *IEEE Trans. Geosci. Remote Sensing*, vol. 39, pp. 2527-2537, Nov. 2001.

[10] M. Bertero and P. Boccacci, *Introduction to Inverse Problems in Imaging*. IOP Publishing Ltd, Bristol, 1998.

[11] M. Donelli and A. Massa, "Computational approach based on a particle swarm optimizer for microwave imaging of two-dimensional dielectric scatterers," *IEEE Trans. Microwave Theory Tech.*, vol. 53, pp. 1761-1776, May 2005.

[12] S. Caorsi, G. L. Gragnani, and M. Pastorino, "An electromagnetic imaging approach using a multi-illumination technique," *IEEE Trans. Biomedical Eng.*, vol. 41, no. 4, pp. 406-409, 1994.

[13] S. Caorsi, G. L. Gragnani, and M. Pastorino, "A multiview microwave imaging system for two- dimensional penetrable objects," *IEEE Trans. Microwave Theory Techn.*, vol. 39, pp. 845-851, May 1991.

[14] W. C. Chew and J. H. Lin, "A Frequency-Hopping Approach for Microwave Imaging of Large Inhomogeneous Bodies," *IEEE Microwave Guided Wave Lett.*, vol. 5, pp. 439-441, Dec. 1995.

[15] O. M. Bucci and T. Isernia, "Electromagnetic inverse scattering: Retrievable information and measurement strategies," *Radio Sci.*, vol. 32, pp. 2123-2138, Nov.-Dec. 1997.

[16] S. Caorsi, G. L. Gragnani, and M. Pastorino, "A model-driven approach to microwave diagnostics in biomedical applications," *IEEE Trans. Microwave Theory Tech.*, vol. 44, no. 10, pp. 1910-1920, Oct. 1996.

[17] D. T. Davis, J. N. Hwang, and L. Tsang, "Solving inverse problems using Bayesian modeling to incorporate information sources," *Geoscience and Remote Sensing Symposium*, 1994.

[18] T. Isernia, V. Pascazio, and R. Pierri, "On the local minima in a tomographic imaging technique," *IEEE Trans. Geosci. Remote Sensing*, vol. 39, pp. 1596-1607, Jul. 2001.

[19] E. L. Miller and A. Willsky, "A multiscale, statistically based inversion scheme for linearized inverse scattering problems," *IEEE Trans. Geosci. Remote Sensing*, vol. 34, pp. 346-357, Mar. 1996.

[20] E. L. Miller, "Statistically based methods for anomaly characterization in images from observations of scattered fields," *IEEE Trans. Image Processing*, vol. 8, pp. 92-101, Jan. 1999.

[21] S. Caorsi, M. Donelli, D. Franceschini, and A. Massa, "A new methodology based on an iterative multiscaling for microwave imaging," *IEEE Trans. Microwave Theory Tech.*, vol. 51, app. 1162-1173, Apr. 2003.

[22] S Caorsi, M. Donelli, and A. Massa, "Detection, location, and imaging of multiple scatterers by means of the iterative multiscaling method," *IEEE Trans. Microwave Theory Tech.*, vol. 52, pp. 1217-1228, Apr. 2004.

[23] A. Baussard, E. L. Miller, and D. Lesselier, "Adaptive multiscale approach for 2D microwave tomography," *URSI - International Symposium on Electromagnetic Theory*, Pisa, Italia, pp. 1092-1094, May 2004.

[24] E. L. Miller, I. Yavuz, L. Nicolaides, and A. Mandelis, "An adaptive multiscale inverse scattering approach to photothermal depth profilometry," *Circuits, Systems, and Signal Process*ing, vol. 19, pp. 339-363, Aug. 2000.

[25] A. Baussard, E. L. Miller, and D. Lesselier, "Adaptive multiscale reconstruction of buried objects," *Inverse Problems*, Special section on "Electromagnetic characterization of buried obstacles", W. C. Chew and D. Lesselier eds., vol. 20, pp. S1-S15, 2004.

[26] E. Wolf, "Determination of the amplitude and the phase of scattered fields by holography," *J. Opt. Soc. Am. A*, vol. 60, pp. 18-20, 1970.

[27] G. W. Faris and H. M. Hertz, "Tunable differential interferometer for optical tomography," *Appl. Opt.*, vol. 28, pp. 4662-4667, 1989.

[28] M. H. Maleki, A. J. Devaney, and A. Schatzberg, "Tomographic reconstruction from optical scattered intensities," *J. Opt. Soc. Am. A*, vol. 9, pp. 1356-1363, 1992.

[29] T. Takenaka, D. J. N. Wall, H. Harada, and M. Tanaka, "Reconstruction algorithm of the refractive index of a cylindrical object from the intensity measurements of the total field," *Microwave Optical Technol. Lett.*, vol. 14, pp. 182-188, Feb. 1997.

[30] M. Lambert and D. Lesselier, "Binary-constrained inversion of a buried cylindrical obstacle from complete and phaseless magnetic fields," *Inverse Problems*, vol. 16, pp. 563-576, 2000.

[31] S. Caorsi, A. Massa, M. Pastorino, and A. Randazzo, "Electromagnetic detection of dielectric scatterers using phaseless synthetic and real data and the memetic algorithm," *IEEE Trans. Geosci. Remote Sensing*, vol. 41, pp. 2745-2753, Dec. 2003.

[32] M. H. Maleki, A. J. Devaney, and A. Schatzberg, "Phase retrieval and intensity-only reconstruction algorithms from optical diffraction tomography," *J. Opt. Soc. Am. A*, vol. 10, pp. 1086-1092, 1993.

[33] L. Crocco, M. D'Urso, and T. Isernia, "Inverse scattering from phaseless measurements of the total field on a closed curve," *J. Opt. Soc. Am. A*, vol. 21, Apr. 2004.

[34] J. H. Richmond, "Scattering by a dielectric cylinder of arbitrary cross section shape," *IEEE Trans. Antennas Propagat.*, vol. 13, pp. 334-341, May 1965.

[35] K. Belkebir and M. Saillard, Special issue on "Testing inversion algorithms against experimental data," *Inverse Problems*, vol. 17, pp. 1565-1702, 2001.

[36] K. Belkebir and M. Saillard, Special issue on "Testing inversion algorithms against experimental data: inhomogeneous targets," *Inverse Problems*, vol. 21, pp. 1-3, 2005.

[37] D. Franceschini, M. Donelli, and A Massa, "Testing the iterative multiscaling method against experimental data - On the effects of the electromagnetic source modeling in the reconstruction process," submitted to *Radio Sci.*, 2005.

[38] F. Natterer, "Numerical treatment of ill-posed problems," in *Inverse Problems*, Ed. G. Talenti, *Lecture Notes in Mathematics*, p. 1225, 1986.

[39] J. Kennedy, R. C. Eberhart, and Y. Shi, *Swarm Intelligence.* San Francisco: Morgan Kaufmann Publishiers, 2001.

[40] J. R. Robinson and Y. Rahmat-Sami, "Particle swarm optimization in electromagnetics," *IEEE Trans. Antennas Propagat.*, vol. 52, pp. 771-778, Mar. 2004.

[41] J.-M. Geffrin, P. Sabouroux, and C. Eyraud, "Free-space experimental scattering database continuation: experimental set-up and measurement precision," *Inverse Problems*, vol. 21, pp. 117-130, 2005.

Figure Captions

- **Figure 1.** Problem geometry.

- **Figure 2.** Block diagram of the *Two-Step* reconstruction Strategy.

- **Figure 3.** Centered square dielectric cylinder ($L_{ref} = \frac{\lambda}{2}$, $\tau_{ref} = 1.0$) - Weighting source coefficients A_w, $w = 1, ..., W$ of the *DCW-Model* ($W = 15$): (a) amplitude and (b) phase.

- **Figure 4.** Centered square dielectric cylinder ($L_{ref} = \frac{\lambda}{2}$, $\tau_{ref} = 1.0$) - Comparison between the incident field measured in D_{obs} and the numerically-computed values of $E_{inc}^v \left(x_{m(v)}, y_{m(v)} \right)$: ($a$) amplitude and ($b$) phase ($v = 1$).

- **Figure 5.** Centered square dielectric cylinder ($L_{ref} = \frac{\lambda}{2}$, $\tau_{ref} = 1.0$) - Actual dielectric profile (a). *PD Approach* - Reconstructed profiles at (b) $s = 1$, (c) $s = 2$, and (d) at the convergence step ($s = 3$) of the *IMSA-PSO Strategy*. *FD Approach* - Reconstructed profiles at the convergence step ($s = 3$) of the *IMSA-PSO Strategy* (e).

- **Figure 6.** Centered square dielectric cylinder ($L_{ref} = \frac{\lambda}{2}$, $\tau_{ref} = 1.0$) - Comparison between actual, estimated with *FD* approach, and *PD* approach values of (a) amplitude and (b) phase of $E_{scatt}^v \left(x_{m(v)}, y_{m(v)} \right)$ in D_{obs}.

- **Figure 7.** Centered square dielectric cylinder ($L_{ref} = \frac{\lambda}{2}$, $\tau_{ref} = 1.0$) - (a) Amplitudes of the actual $E_{tot}^v \left(x_{m(v)}, y_{m(v)} \right)$ and reconstructed $\xi_{tot}^v \left(x_{m(v)}, y_{m(v)} \right)$ total field in D_{obs}. (b) Amplitudes of the actual $E_{inc}^v \left(x_{n(r)}, y_{n(r)} \right)$, estimated $\widetilde{E_{inc}^v} \left(x_{n(r)}, y_{n(r)} \right)$, and reconstructed $\xi_{inc}^v \left(x_{n(r)}, y_{n(r)} \right)$ incident field in D_{inv}.

- **Figure 8.** Centered square dielectric cylinder ($L_{ref} = \frac{\lambda}{2}$, $\tau_{ref} = 1.0$) - Comparison between *PD Approach* and *FD Approach* (*IMSA-PSO Strategy*) in terms of error figures: (a) ρ, (b) Δ, (c) γ_{tot}, (d) γ_{int} and (e) γ_{ext}.

- **Figure 9.** Two square lossy cylinders ($L_{ref}^{(1)} = \frac{\lambda}{4}$, $\tau_{ref}^{(1)} = 3.0 - j0.4$ and $L_{ref}^{(2)} = \frac{\lambda}{2}$, $\tau_{ref}^{(2)} = 1.5 - j0.25$ - $SNR = 20\,dB$) - Actual dielectric profile: (a) $Re\left\{ \tau_{ref}(x,y) \right\}$ and (b) $Im\left\{ \tau_{ref}(x,y) \right\}$. *PD Approach* - Reconstructed profiles at the convergence

step ($s = 3$) of the *IMSA-PSO Strategy*: (*c*) $Re \{\tau(x, y)\}$ and (*d*) $Im \{\tau(x, y)\}$. *FD Approach* - Reconstructed profiles at the convergence step ($s = 2$) of the *IMSA-PSO Strategy*: (*e*) $Re \{\tau(x, y)\}$ and (*f*) $Im \{\tau(x, y)\}$.

- **Figure 10.** Off-centered homogeneous circular dielectric cylinder (Real dataset [35] "*dielTM_ dec8f.exp*" - $f = 1\, GHz$). *PD Approach* - Reconstructed profiles with (*a*) "*bare*" *PSO-based Approach* and (*b*) *IMSA-PSO Strategy*. *FD Approach* - Reconstructed profiles with (*c*) "*bare*" *PSO-based Approach*, (*d*) *IMSA-PSO Strategy*, (*e*) "*bare*" *CG-based Approach*, and (*f*) *IMSA-CG Strategy*.

- **Figure 11.** Off-centered homogeneous circular dielectric cylinder (Real dataset [35] "*dielTM_ dec8f.exp*" - $f = 1\, GHz$) - (*a*) Amplitudes of the actual $E_{tot}^{v}\left(x_{m(v)},\, y_{m(v)}\right)$ and reconstructed $\xi_{tot}^{v}\left(x_{m(v)},\, y_{m(v)}\right)$ total field in D_{obs}. (*b*) Amplitudes of the estimated $\widetilde{E_{inc}^{v}}\left(x_{n(r)},\, y_{n(r)}\right)$ and reconstructed $\xi_{inc}^{v}\left(x_{n(r)},\, y_{n(r)}\right)$ incident field in D_{inv}.

- **Figure 12.** Off-centered homogeneous circular dielectric cylinder (Real dataset [35] "*dielTM_ dec8f.exp*" - $f = 1\, GHz$) - Comparison between actual, estimated with *FD* approach, and *PD* approach values of (*a*) amplitude and (*b*) phase of $E_{scatt}^{v}\left(x_{m(v)},\, y_{m(v)}\right)$ in D_{obs}.

- **Figure 13.** Off-centered homogeneous circular dielectric cylinder (Real dataset [35] "*dielTM_ dec8f.exp*") - Behavior of the localization error ρ versus frequency.

- **Figure 14.** Multi-layer dielectric circular cylinder (Real dataset [36] "*FoamDielIntTM*" - $f = 2GHz$) - Comparison between the incident field measured in D_{obs} and the numerically-computed values of $E_{inc}^{v}\left(x_{m(v)}, y_{m(v)}\right)$: (*a*) amplitude and (*b*) phase ($v = 1$).

- **Figure 15.** Multi-layer dielectric circular cylinder (Real dataset [36] "*FoamDielIntTM*" - $f = 2GHz$). *PD Approach* - Reconstructed profiles with (*a*) "*bare*" *PSO-based Approach* and (*b*) *IMSA-PSO Strategy*. *FD Approach* - Reconstructed profiles with (*c*) "*bare*" *PSO-based Approach* and (*d*) *IMSA-PSO Strategy*.

Table Captions

- **Table I.** Centered square dielectric cylinder ($L_{ref} = \frac{\lambda}{2}$, $\tau_{ref} = 1.0$) - Values of the qualitative (ρ and δ) and quantitative (γ_{tot}, γ_{int}, and γ_{ext}) error figures at different steps s ($s = 1, 2, 3$) of the *IMSA-PSO* strategy for the *FD* and *PD* approach, respectively.

- **Table II.** Off-centered homogeneous circular dielectric cylinder (Real dataset [35] "*dielTM_ dec8f.exp*" - $f = 1\,GHz$) - Location and shape parameters.

- **Table III.** Multi-layer dielectric circular cylinder (Real dataset [36] "*FoamDielIntTM*" - $f = 2GHz$) - Location and shape parameters.

$(x_{m(v)}, y_{m(v)})$

Investigation Domain

E_{inc}^v

τ

τ_0

E_{tot}^v

Observation Domain
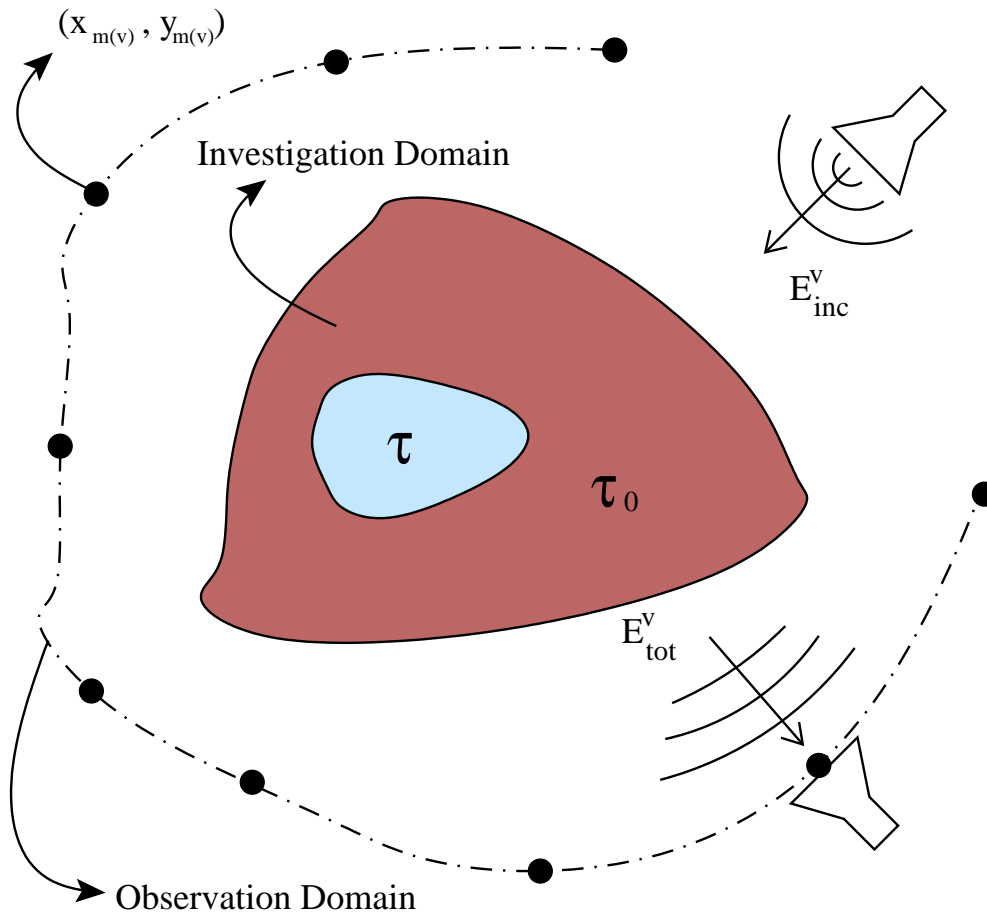
Fig. 1 - G. Franceschini *et al.,* "Inversion of phaseless total field data using ..."
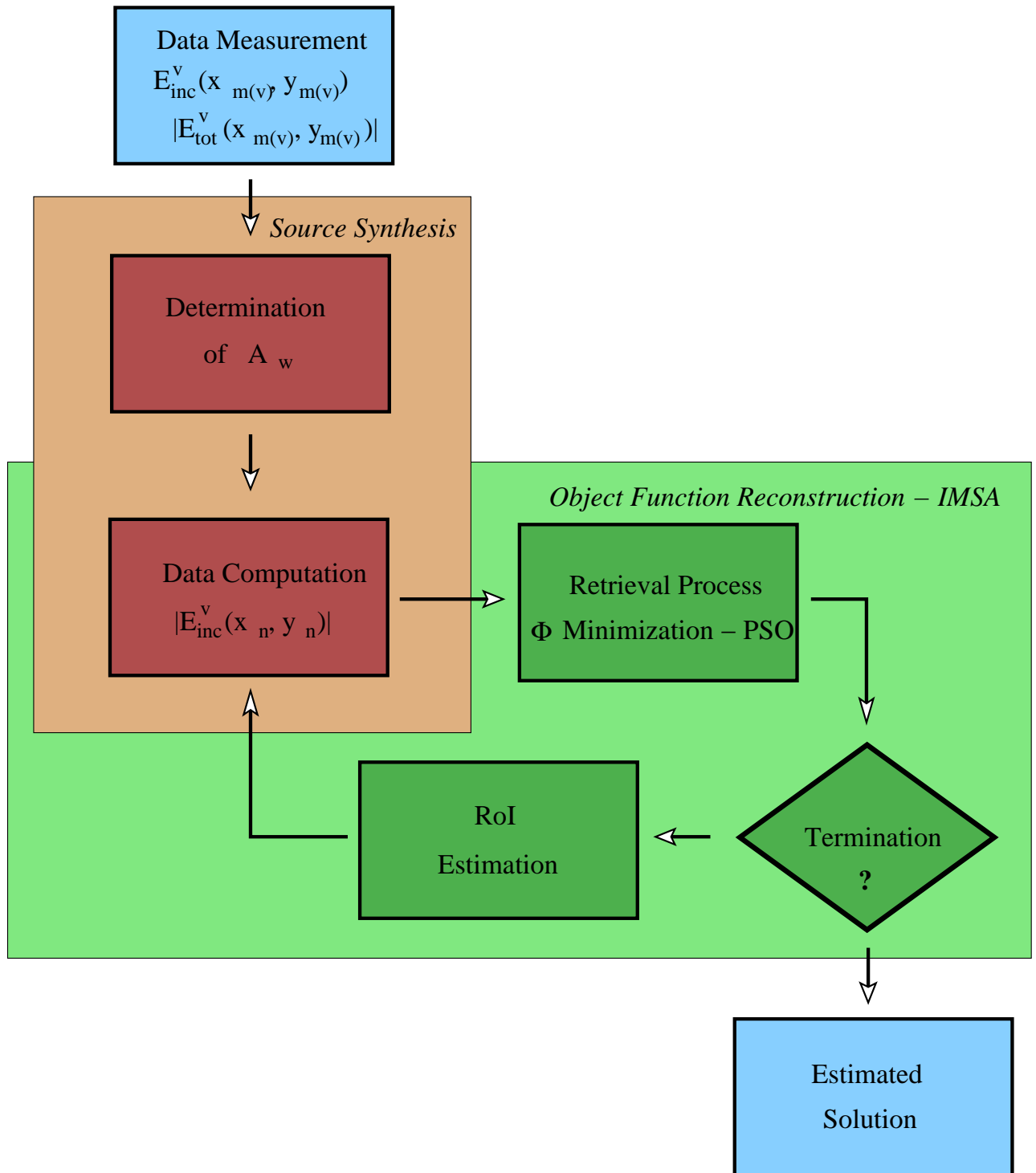
Fig. 2 - G. Franceschini *et al.*, ”Inversion of phaseless total field data using ...”
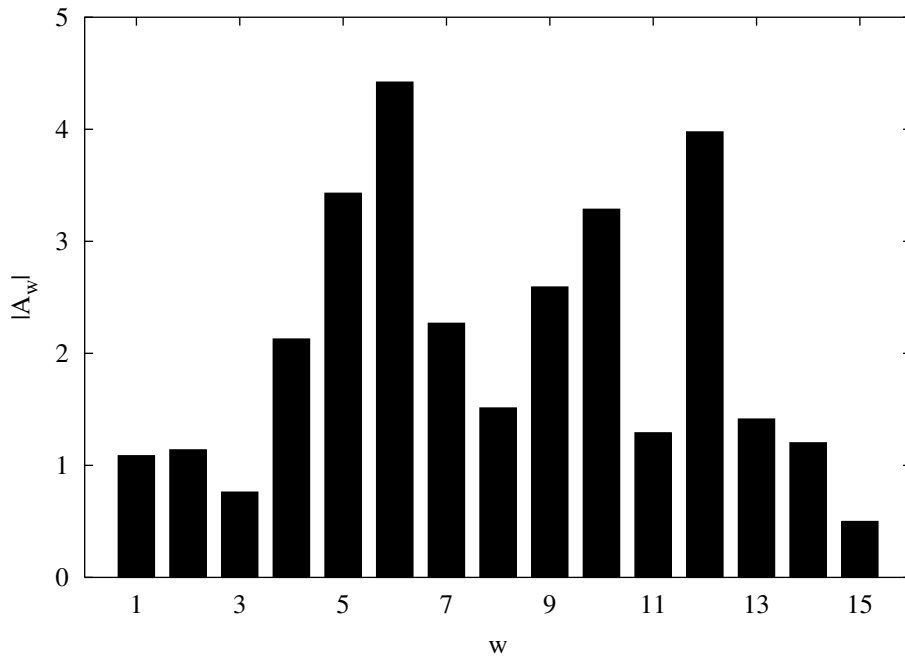
(a)
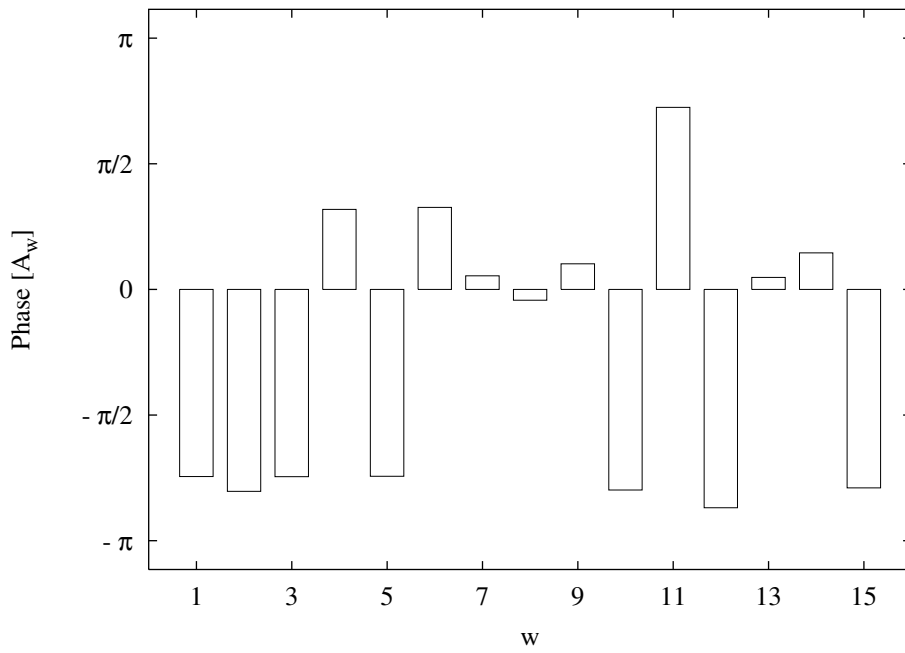
(b)

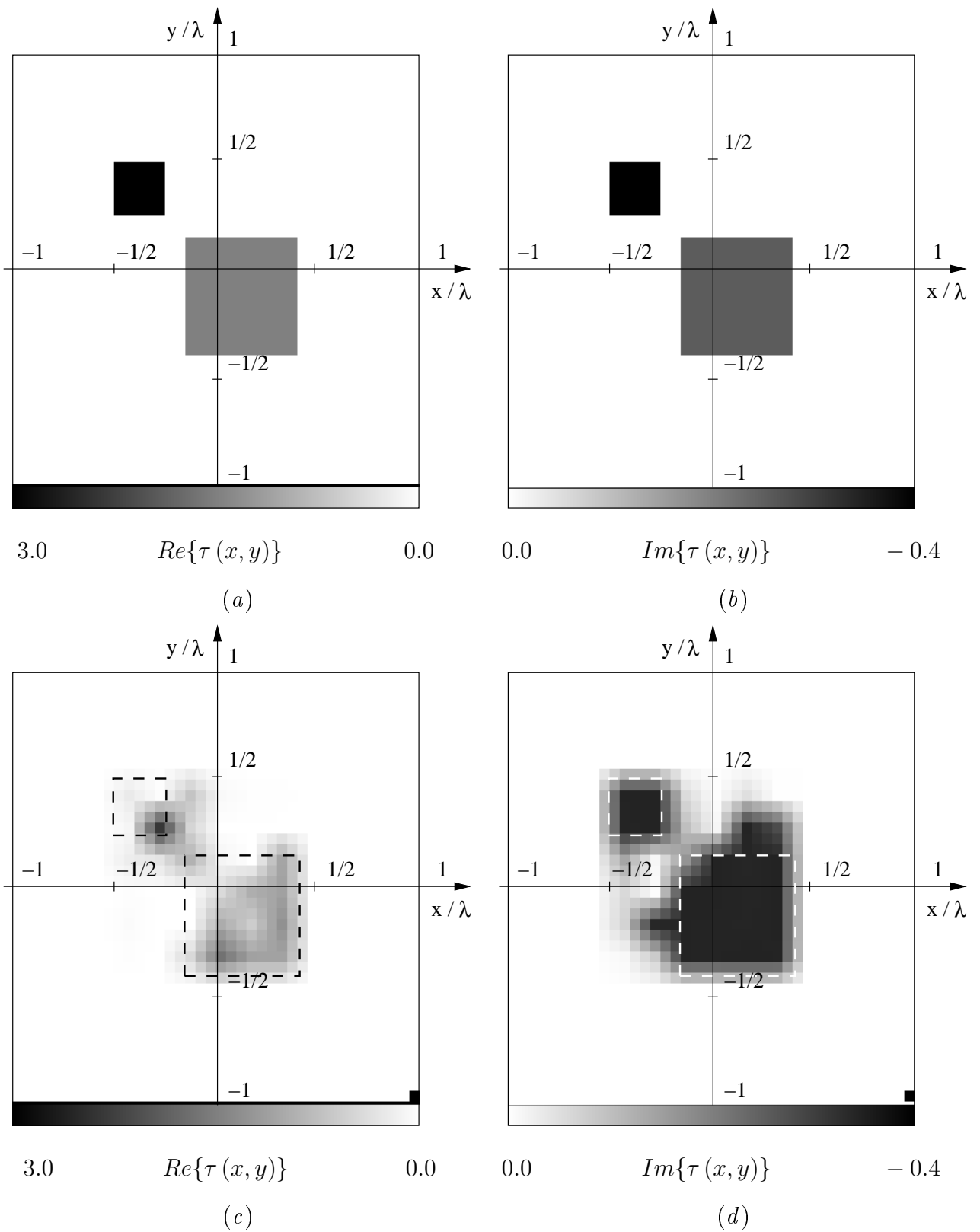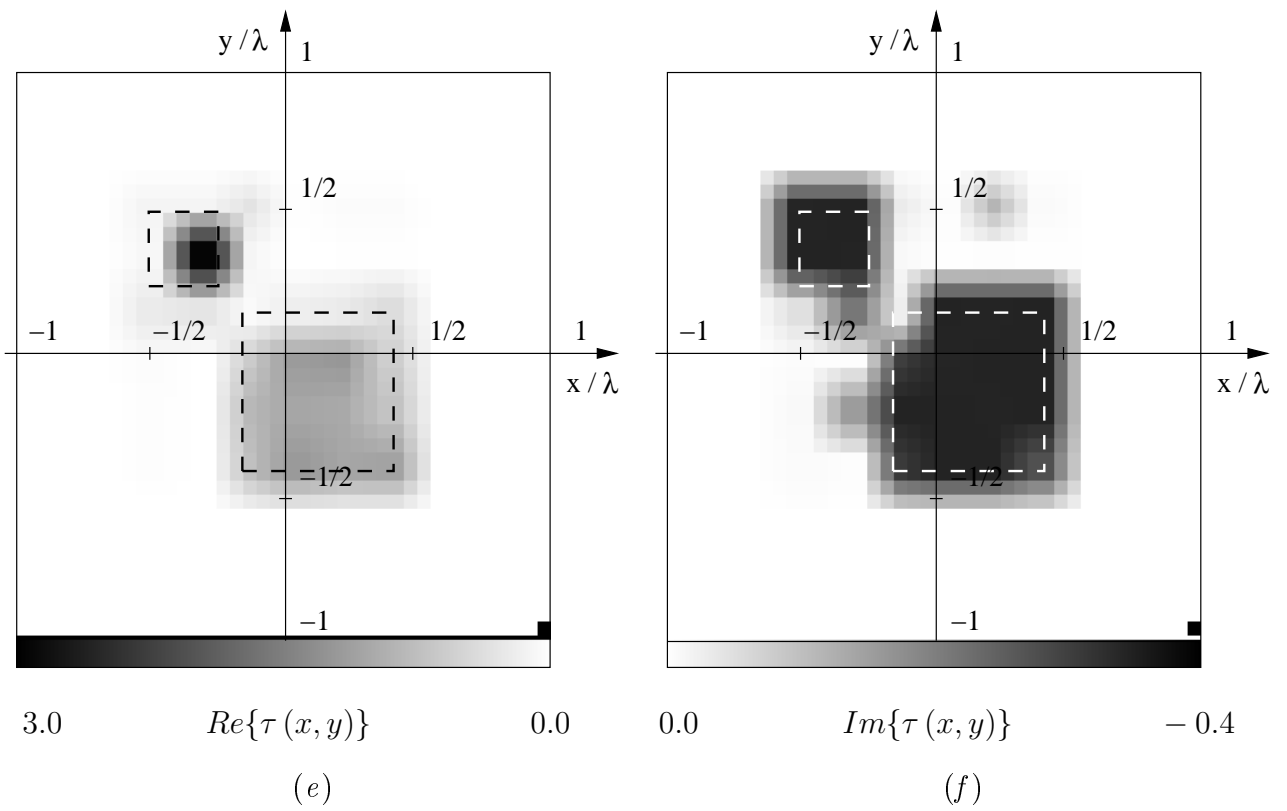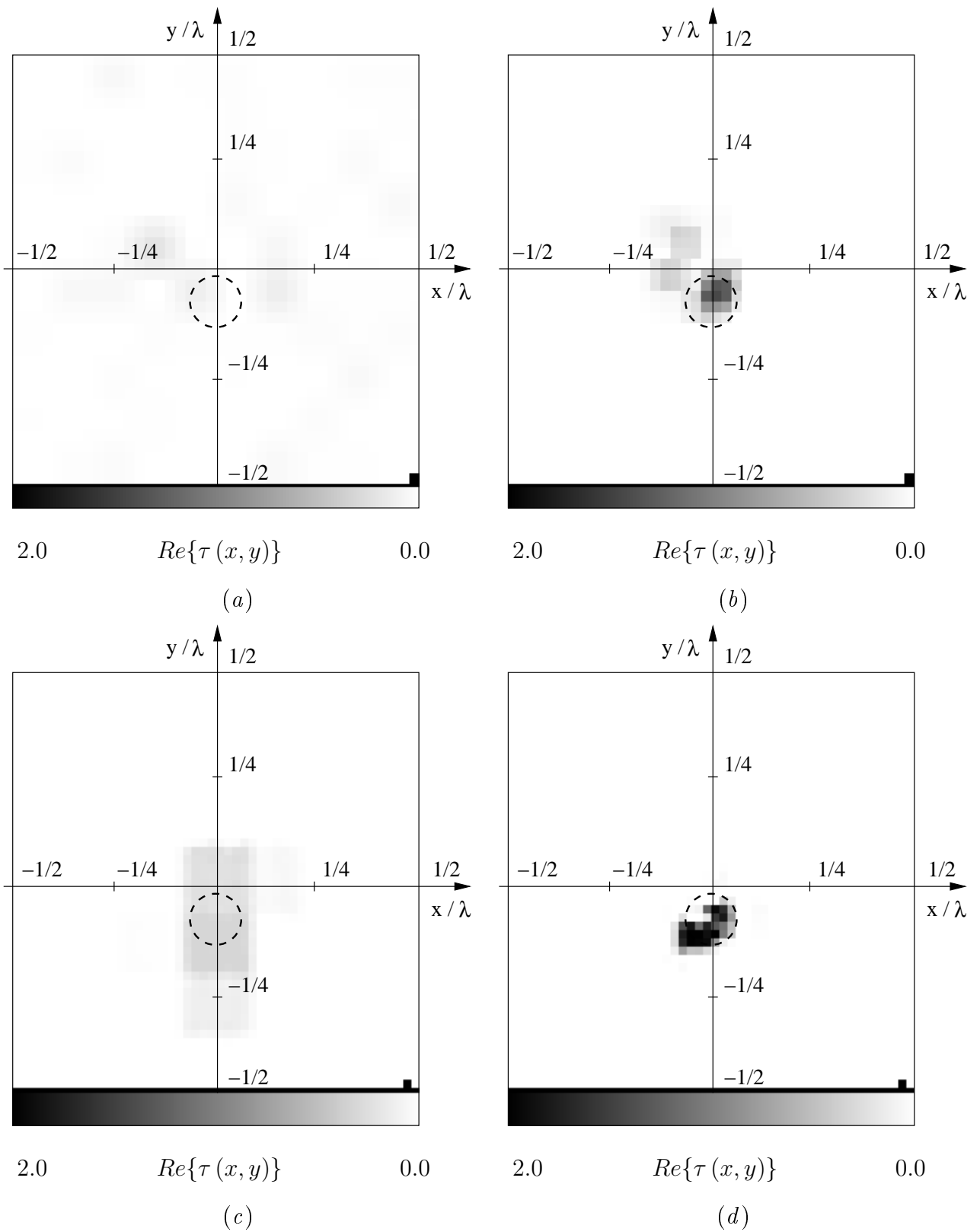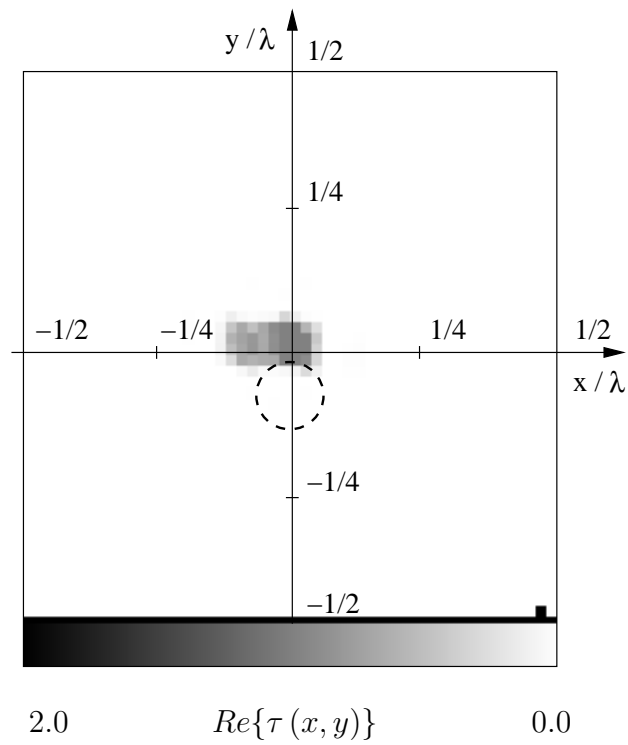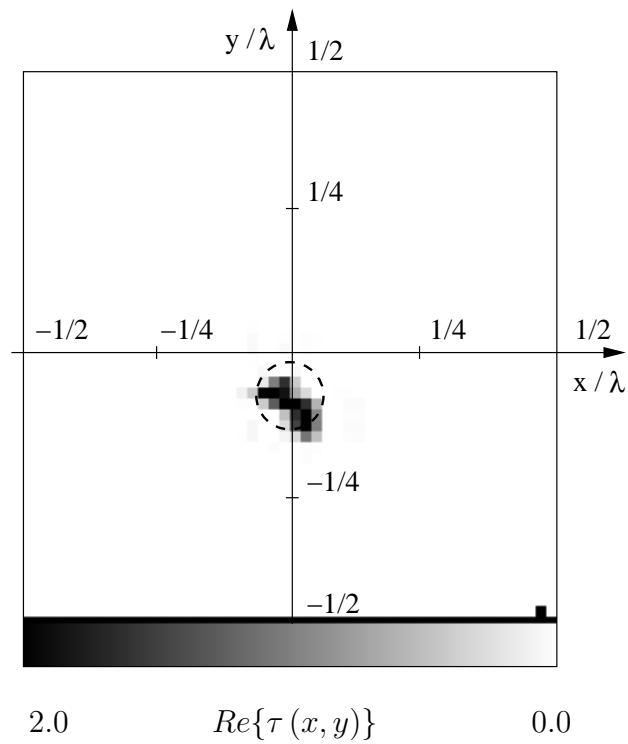**Fig. 3 - G. Franceschini *et al.*,** "Inversion of phaseless total field data using ..."
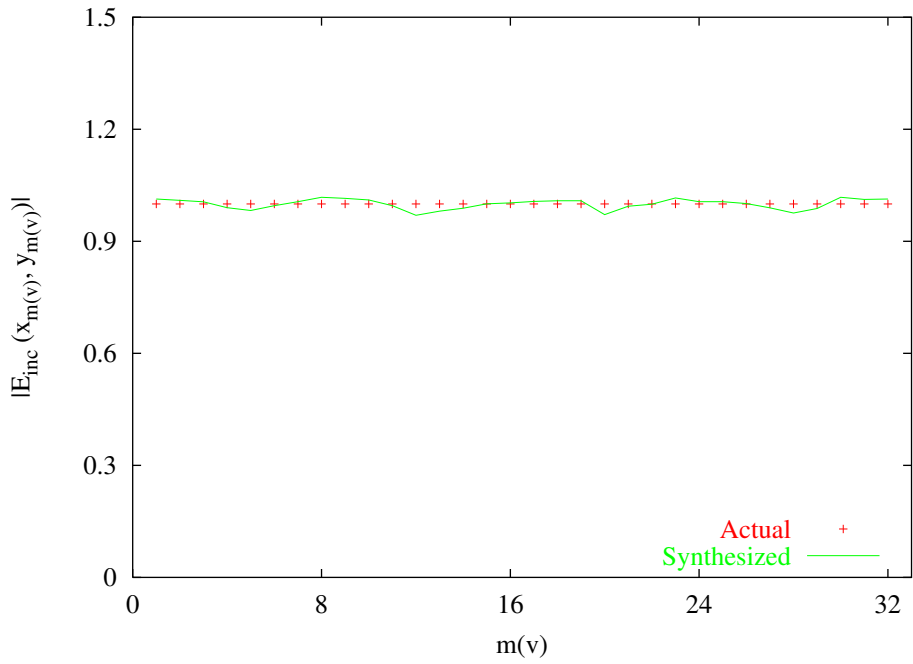
(a)
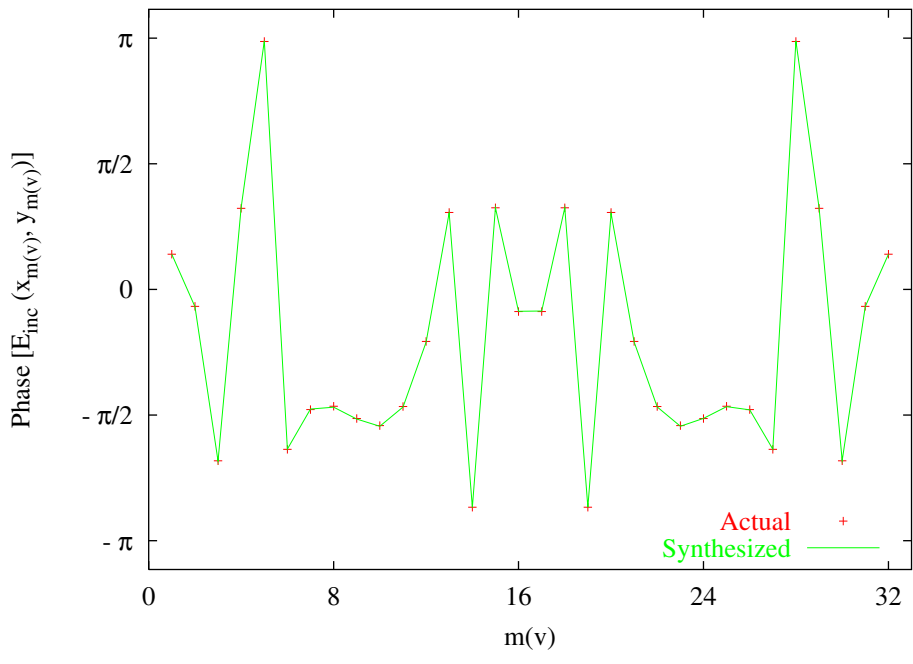
(b)

Fig. 4 - G. Franceschini _et al._, "Inversion of phaseless total field data using ..."

31

(a) (b)

(c) (d)
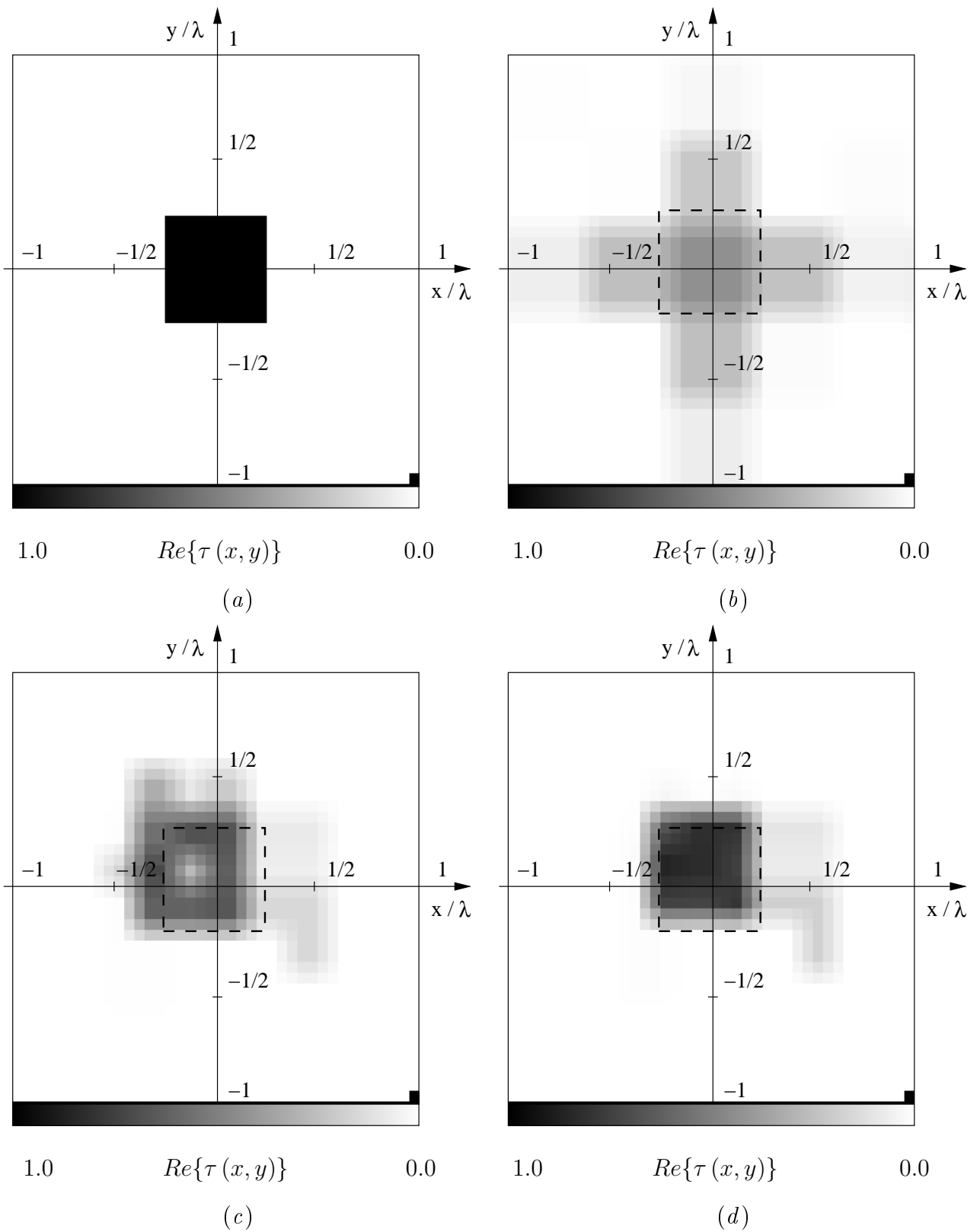
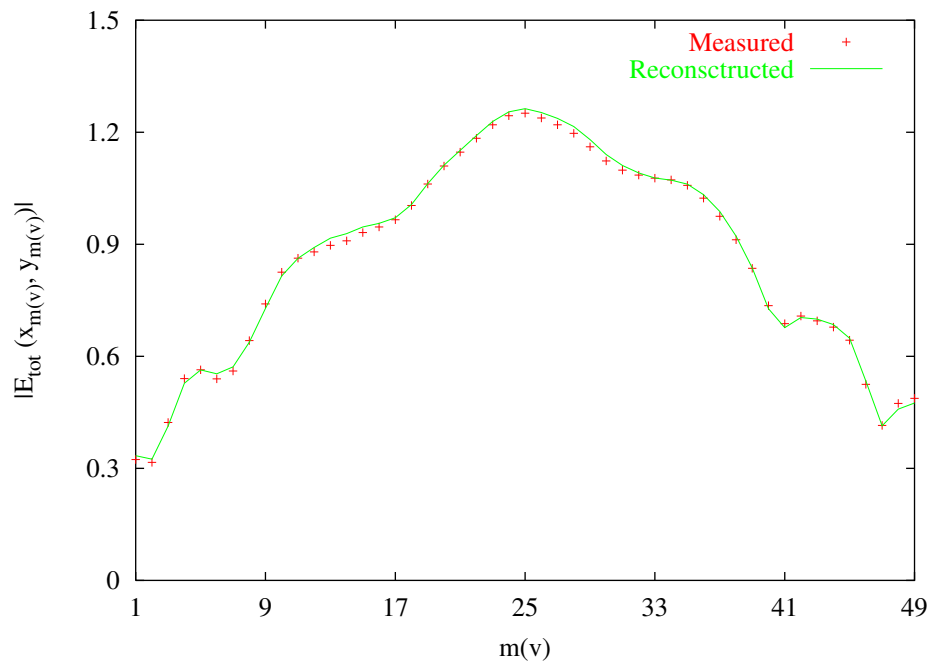**Fig. 5(I) - G. Franceschini *et al.*,** "Inversion of phaseless total field data using ..."
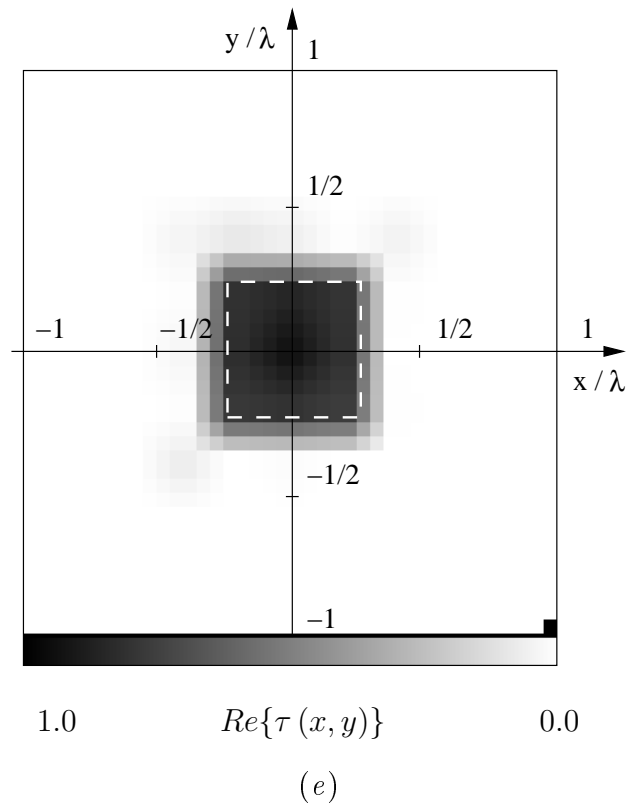
Fig. 5(*II*) - G. Franceschini *et al.*, "Inversion of phaseless total field data using ..."
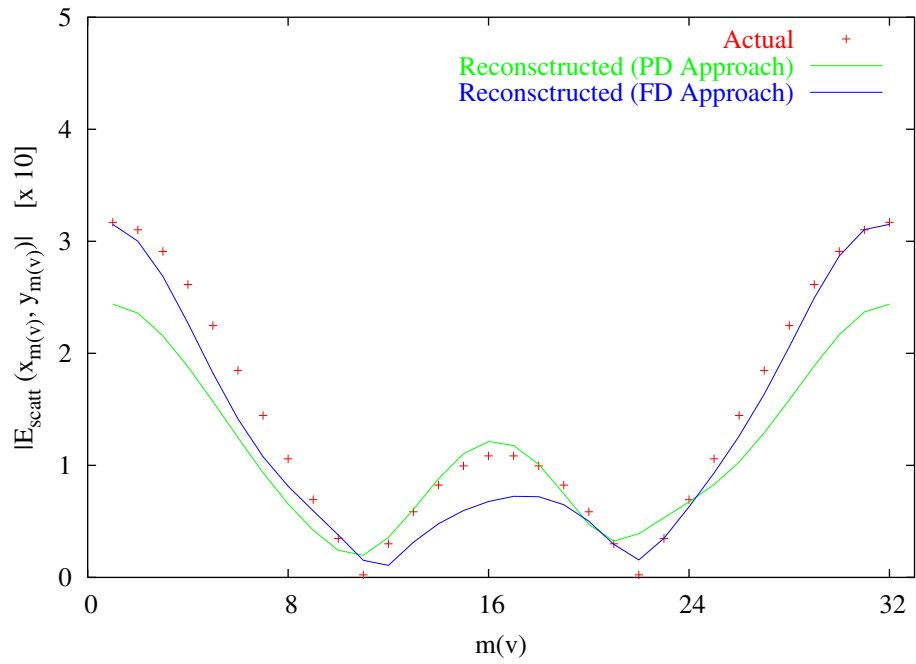
(a)
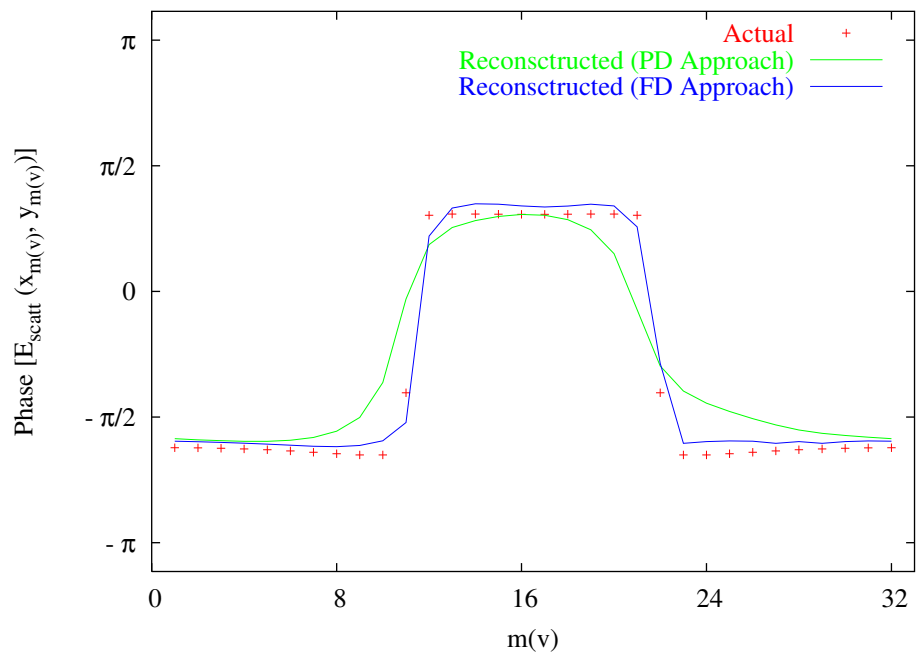
(b)

Fig. 6 - G. Franceschini *et al.*, "Inversion of phaseless total field data using ..."
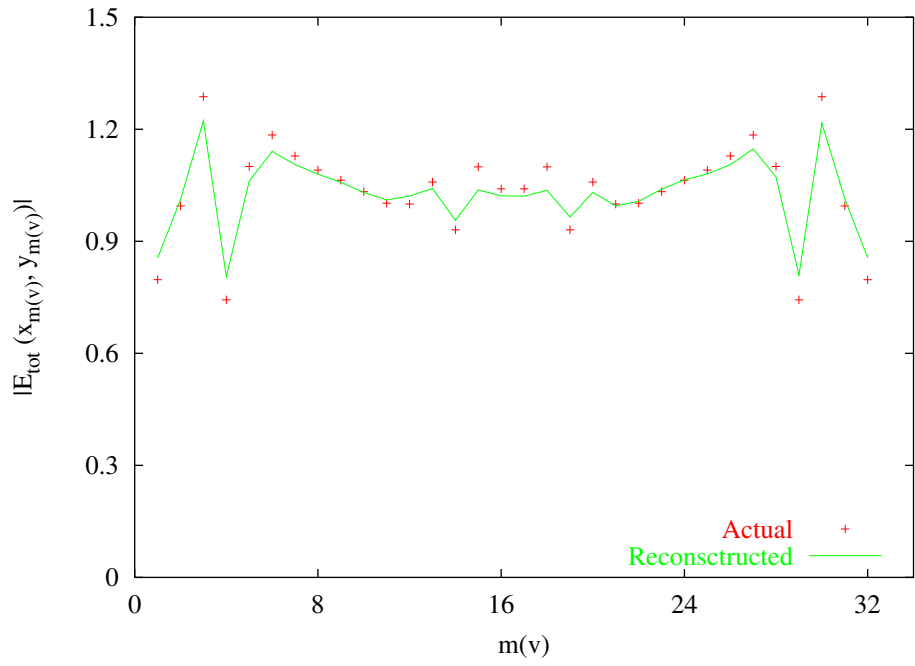
(a)
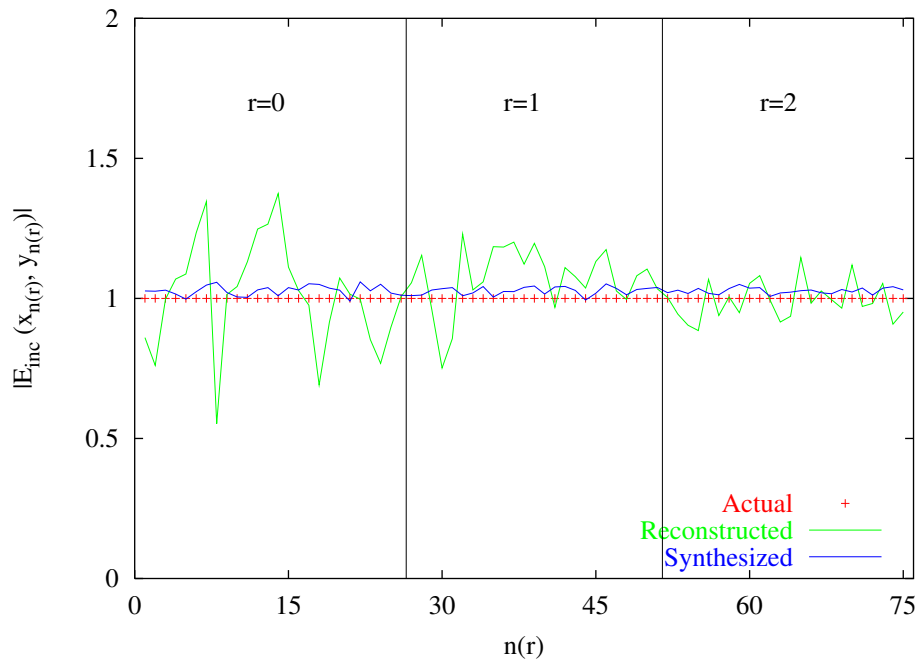
(b)

Fig. 7 - G. Franceschini *et al.*, "Inversion of phaseless total field data using ..."
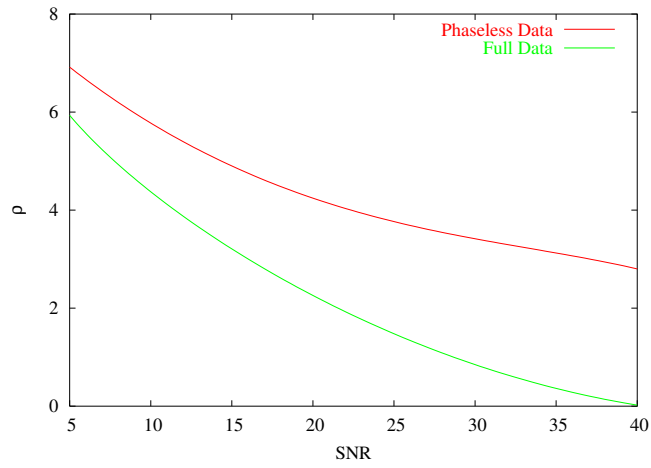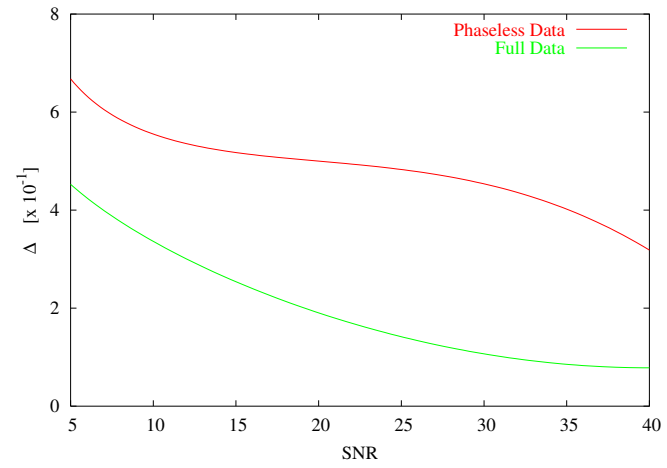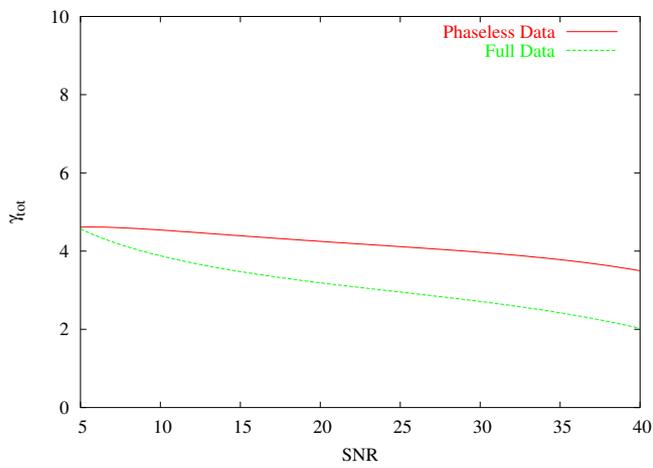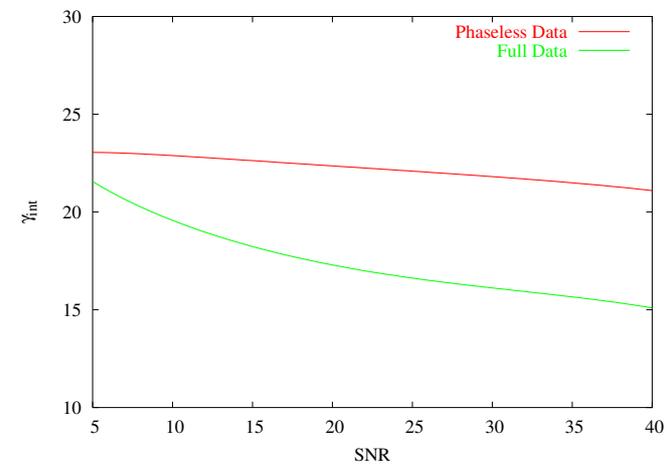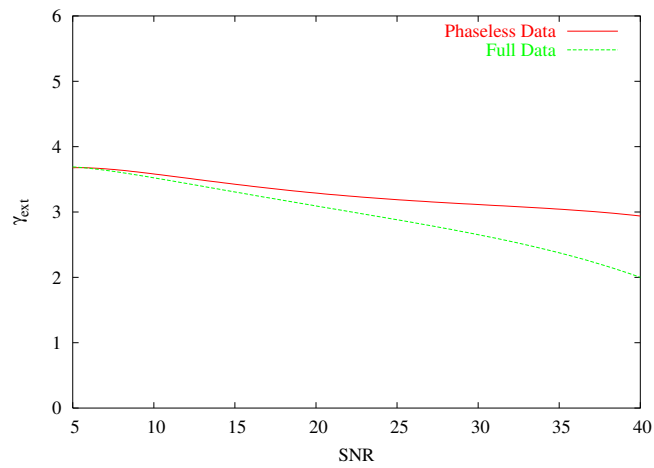
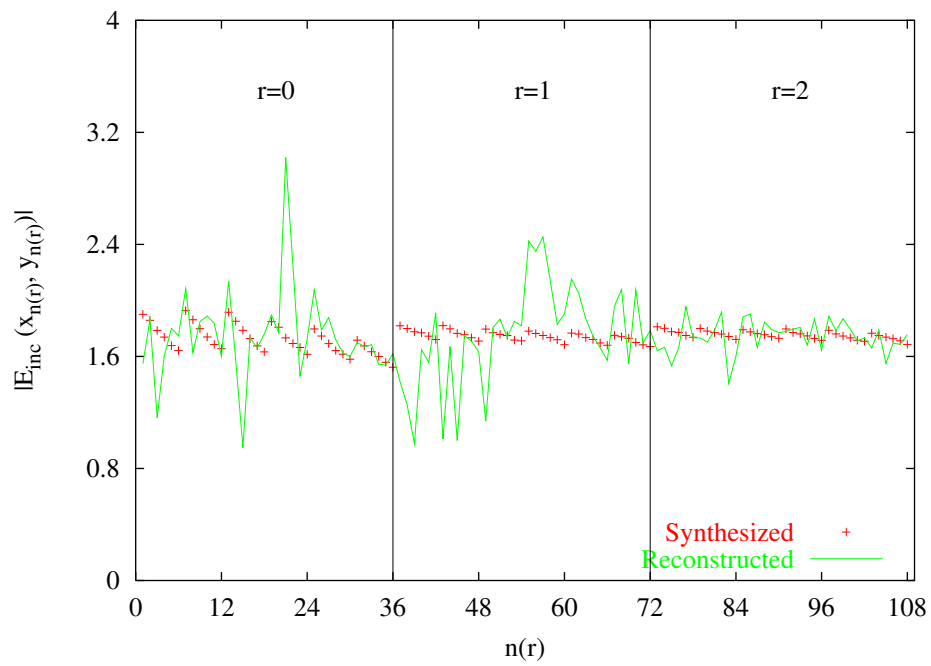Fig. 8 - G. Franceschini *et al.*, "Inversion of phaseless total field data using ..."

Fig. 9(**I**) - G. Franceschini **et al.,** "Inversion of phaseless total field data using ..."

Fig. 9(*II*) - G. Franceschini *et al.*, "Inversion of phaseless total field data using ..."

Fig. 10(I) - G. Franceschini *et al.*, "Inversion of phaseless total field data using ..."

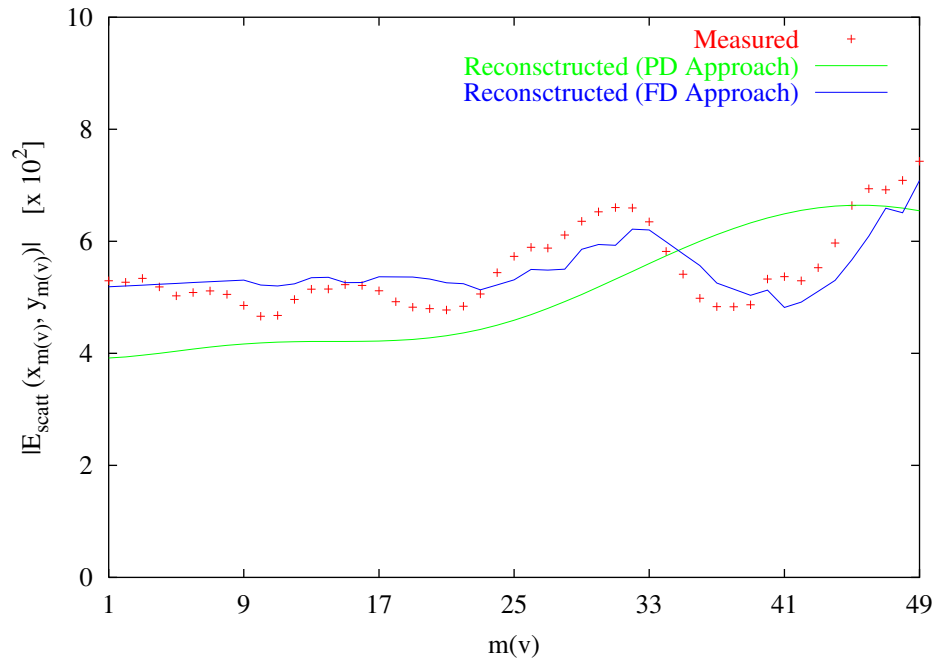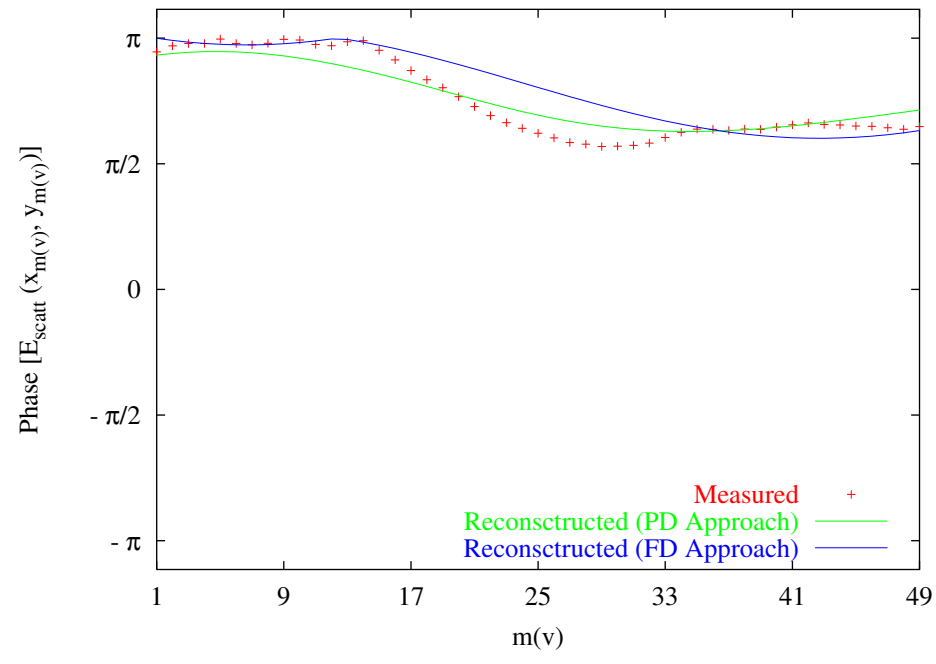**Fig. 10(*II*) - G. Franceschini *et al.*,** "Inversion of phaseless total field data using ..."

(a)

(b)

Fig. 11 - G. Franceschini *et al.*, "Inversion of phaseless total field data using ..."

(a)

(b)

Fig. 12 - G. Franceschini _et al._, "Inversion of phaseless total field data using ..."

(a)

(b)

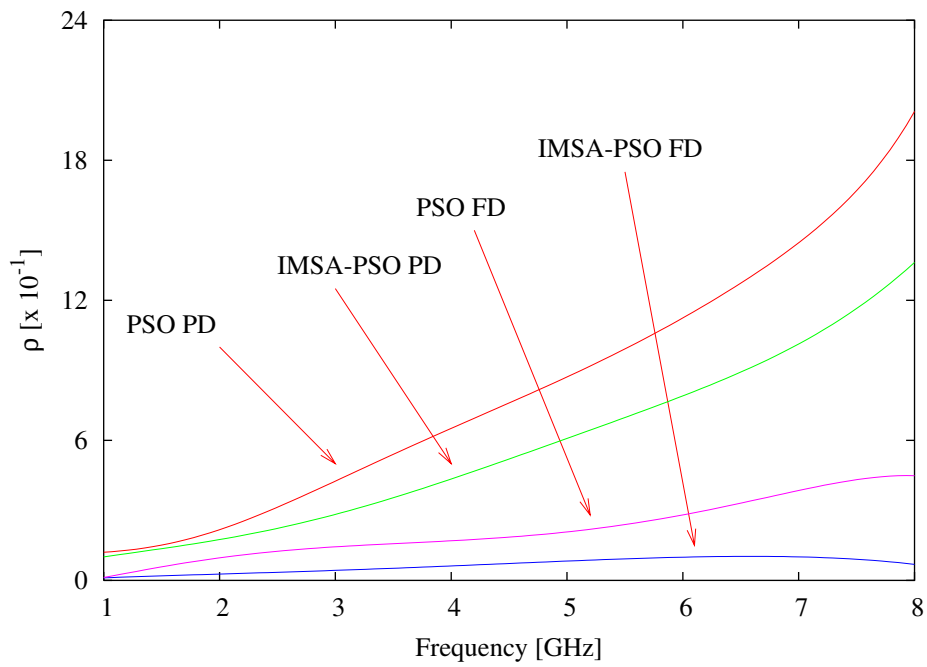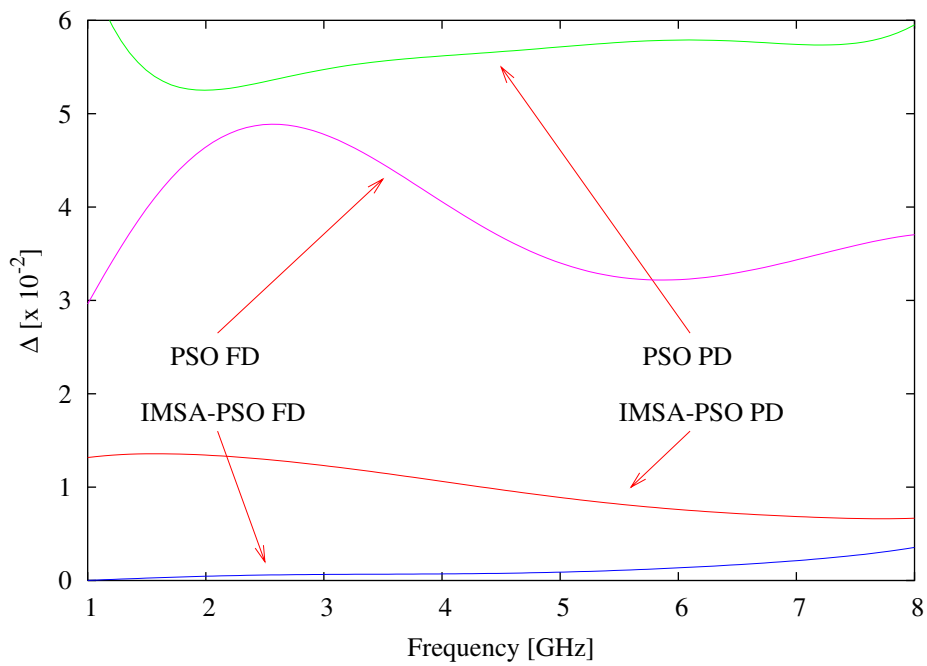**Fig. 13 - G. Franceschini *et al.*,** "Inversion of phaseless total field data using ..."

(a)

(b)

Fig. 14 - G. Franceschini _et al._, "Inversion of phaseless total field data using ..."

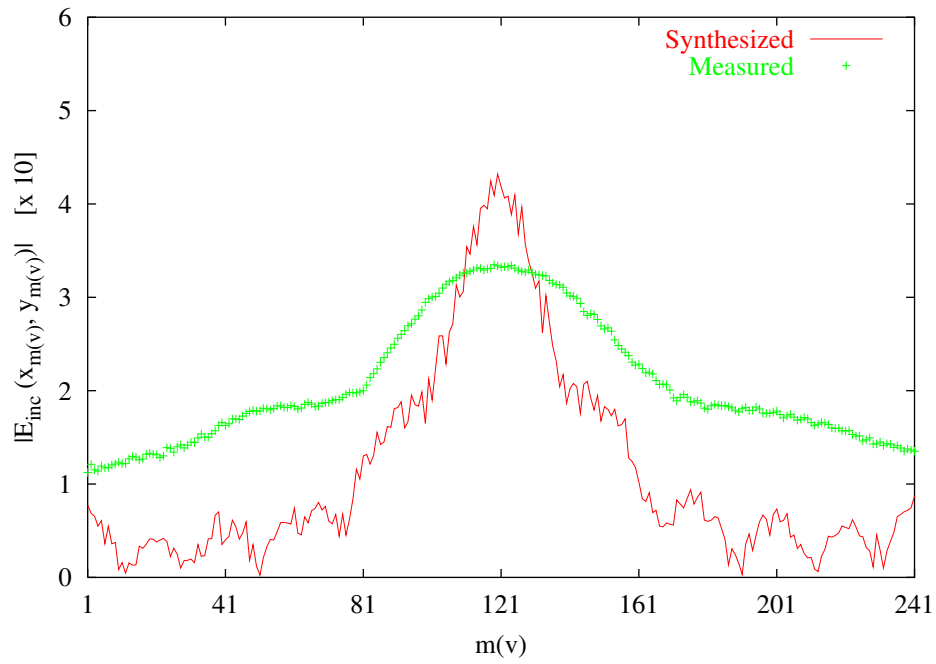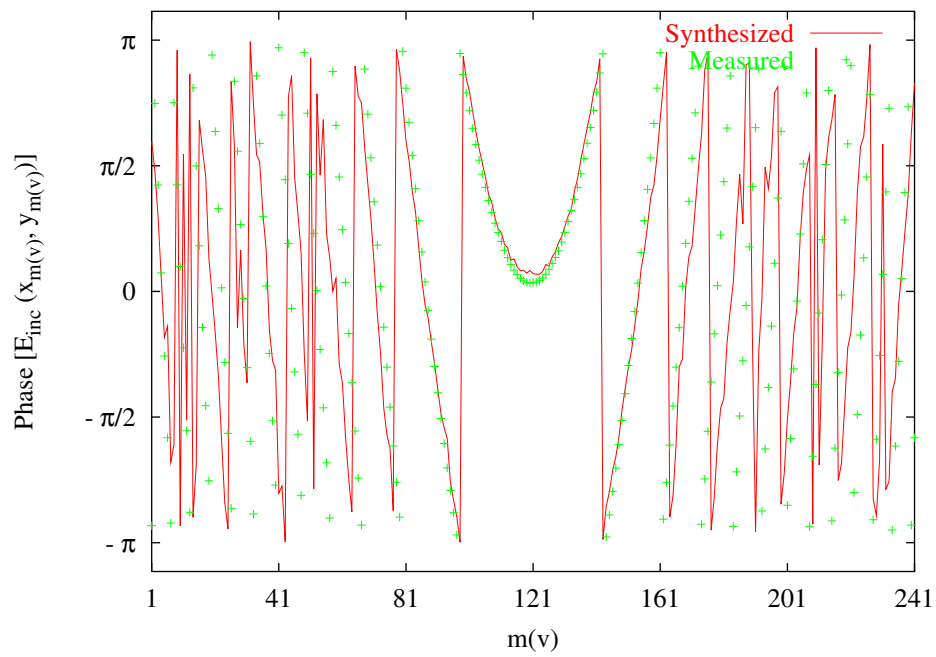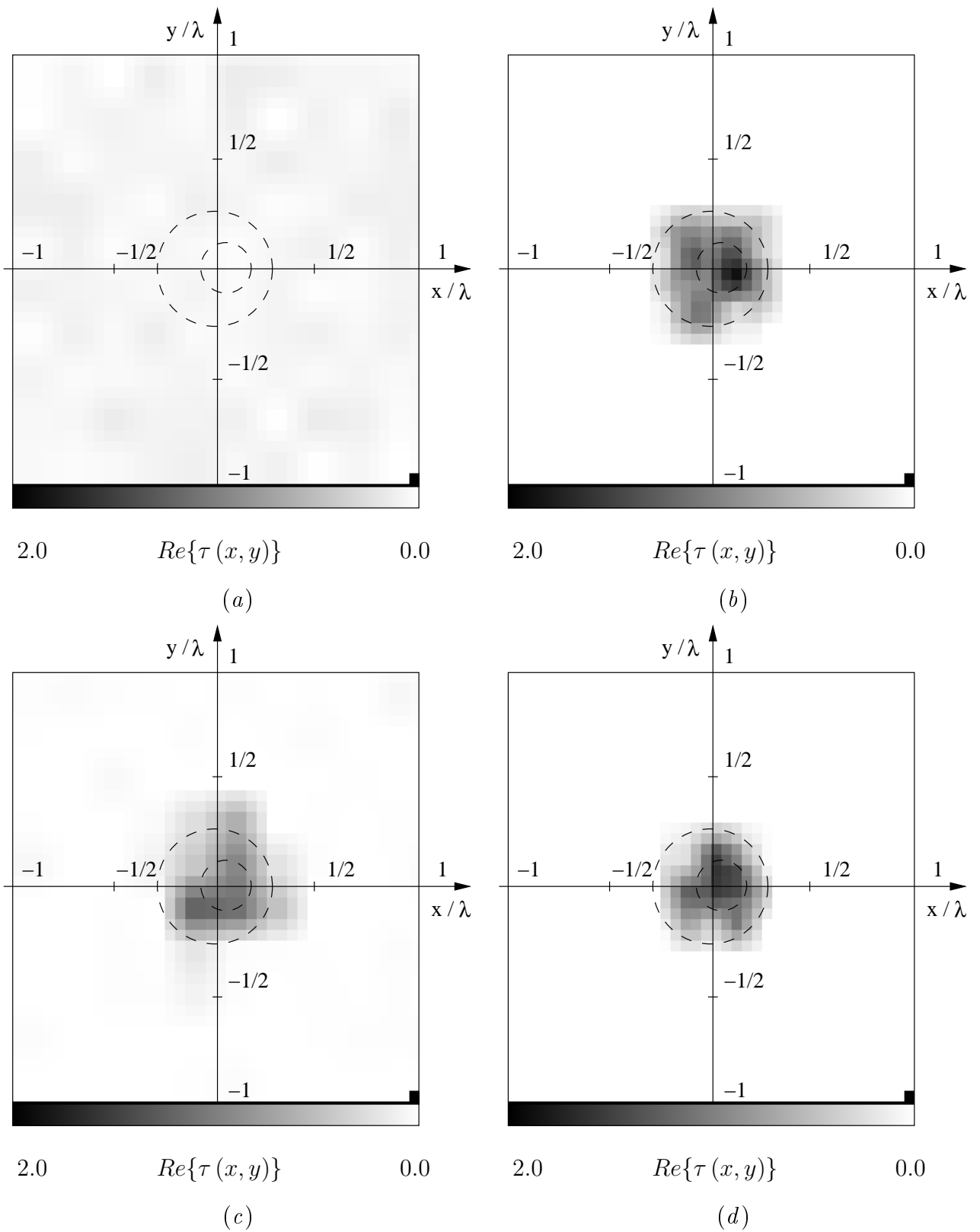**Fig. 15 - G. Franceschini *et al.*,** "Inversion of phaseless total field data using ..."

Step No.	γ_{tot}	γ_{int}	γ_{ext}	ρ	Δ
PD Approach					
$s = 1$	7.25	28.6	5.83	2.65	161
$s = 2$	5.41	22.9	4.25	2.49	44.1
$s = 3$	3.49	21.1	2.32	2.80	31.8
FD Approach					
$s = 1$	8.41	32.8	6.79	1.08	191
$s = 2$	4.19	25.7	2.09	0.82	61.8
$s = 3$	2.02	15.1	2.00	0.02	7.83

Tab. I - G. Franceschini *et al.*, "Inversion of phaseless total field data using ..."

	$\frac{x_{RoI}}{\lambda}$	$\frac{y_{RoI}}{\lambda}$	$\frac{L_{RoI}}{2\lambda}$
Actual Profile			
	0.0	-1.0×10^{-1}	5.0×10^{-2}
Reconstructed Profile (PD Approach)			
PSO	1.3×10^{-2}	-4.0×10^{-4}	2.9×10^{-1}
$IMSA - PSO$	4.3×10^{-3}	-6.0×10^{-2}	1.2×10^{-1}
Reconstructed Profile (FD Approach)			
PSO	7.0×10^{-3}	-1.1×10^{-1}	2.0×10^{-1}
$IMSA - PSO$	6.0×10^{-3}	-1.1×10^{-1}	5.0×10^{-2}
CG	2.3×10^{-2}	-1.3×10^{-1}	1.9×10^{-1}
$IMSA - CG$	-8.7×10^{-3}	-1.0×10^{-1}	1.1×10^{-1}

Tab. II - G. Franceschini *et al.*, "Inversion of phaseless total field data using ..."

	$\frac{x_{RoI}}{\lambda}$	$\frac{y_{RoI}}{\lambda}$	$\frac{L_{RoI}}{2\lambda}$
Actual Profile			
	7.3×10^{-3}	0.0	2.7×10^{-1}
Reconstructed Profile (PD Approach)			
PSO	2.5×10^{-2}	1.3×10^{-3}	8.7×10^{-1}
IMSA − PSO	3.5×10^{-2}	-1.3×10^{-2}	2.5×10^{-1}
Reconstructed Profile (FD Approach)			
PSO	3.5×10^{-2}	2.5×10^{-2}	3.0×10^{-1}
IMSA − PSO	3.1×10^{-2}	-8.7×10^{-3}	2.6×10^{-1}

Tab. III - G. Franceschini *et al.*, "Inversion of phaseless total field data using ..."